Published for SISSA by Springer

Received: June 10, 2010
Revised: March 19, 2011
Accepted: May 11, 2011
Published: June 13, 2011

RECO level $\sqrt{s}_{\rm min}$ and subsystem $\sqrt{s}_{\rm min}$: improved global inclusive variables for measuring the new physics mass scale in $\not{E}_T$ events at hadron colliders

Partha Konar,[a,b] **Kyoungchul Kong,**[c,d] **Konstantin T. Matchev**[a] **and Myeonghun Park**[a]

[a] *Physics Department, University of Florida, Gainesville, FL 32611, U.S.A.*

[b] *Theoretical Physics, Physical Research Laboratory, Ahmedabad 380009, India*

[c] *Theoretical Physics Department, SLAC, Menlo Park, CA 94025, U.S.A.*

[d] *Department of Physics, University of Kansas, Lawrence, KS 66045, U.S.A.*

E-mail: konar@phys.ufl.edu, kckong@slac.stanford.edu, matchev@phys.ufl.edu, ishaed@phys.ufl.edu

Abstract: The variable $\sqrt{s}_{\rm min}$ was originally proposed in [1] as a model-independent, global and fully inclusive measure of the new physics mass scale in missing energy events at hadron colliders. In the original incarnation of $\sqrt{s}_{\rm min}$, however, the connection to the new physics mass scale was blurred by the effects of the underlying event, most notably initial state radiation and multiple parton interactions. In this paper we advertize two improved variants of the $\sqrt{s}_{\rm min}$ variable, which overcome this problem. First we show that by evaluating the $\sqrt{s}_{\rm min}$ variable at the RECO level, in terms of the reconstructed objects in the event, the effects from the underlying event are significantly diminished and the nice correlation between the peak in the $\sqrt{s}_{\rm min}^{(reco)}$ distribution and the new physics mass scale is restored. Secondly, the underlying event problem can be avoided altogether when the $\sqrt{s}_{\rm min}$ concept is applied to a subsystem of the event which does not involve any QCD jets. We supply an analytic formula for the resulting subsystem $\sqrt{s}_{\rm min}^{(sub)}$ variable and show that its peak exhibits the usual correlation with the mass scale of the particles produced in the subsystem. Finally, we contrast $\sqrt{s}_{\rm min}$ to other popular inclusive variables such as H_T, M_{Tgen} and M_{TTgen}. We illustrate our discussion with several examples from supersymmetry, and with dilepton events from top quark pair production.

Keywords: Jets, Beyond Standard Model, Supersymmetric Standard Model, Standard Model

ArXiv ePrint: 1006.0653

doi:10.1007/JHEP06(2011)041

JHEP06(2011)041

Contents

JHEP06(2011)041

1 Introduction and motivation

1.1 The need for a universal, global and inclusive mass variable

It is generally believed that missing energy signatures offer the best bet for discovering new physics Beyond the Standard Model (BSM) at colliders. This belief is reinforced by the dark matter puzzle where as the Standard Model (SM) does not provide a suitable dark matter candidate. Dark matter particles being invisible in the detector, lead to missing momentum signature in the detector. Unfortunately, $\not\!\!\vec{P}_T$ is the only measured quantity directly related to the invisible particles at a hadron collider. Without any further model-dependent assumptions, it is in general very difficult if not impossible to make any definitive statements about the nature and properties of the missing particles. For example, leaving all theoretical prejudice aside, one would not be able to answer such basic and fundamental questions like [1–5]: How many invisible particles were produced in the event? Are all invisible particles SM neutrinos, or are there any new neutral, stable, weakly-interacting massive particles (WIMPs) among them? What are the masses of the new invisible particles? What are their spins? What are the masses of any (parent) particles which may have decayed to invisible particles?

The recent literature is abundant with numerous proposals on how *under particular circumstances* one might be able to measure the masses of the invisible particles (see ref. [6] for a recent review.). Unfortunately, all of the proposed methods suffer from varying degrees of model-dependence as follows:

- *Limited applicability topology-wise.* Most methods crucially rely on the assumption of a very specific event topology with a requirement of the identification of symmetric and sufficiently long cascade decay chain (e.g. invariant mass endpoint methods [7–18] and polynomial methods [19–26] requires at least three successive two-body decays [27]). More recent M_{T2} [28–37], and M_{CT} [38–40], methods typically assume the production two same parent particles which decay to two identical invisible particles (see [3, 4] for a more general approach which avoids this assumption.).

- *Limited applicability signature-wise.* The performance of the methods typically deteriorates as we lower the number of isolated leptons in the signature.

- *Combinatorics problem.* This is an inevitable part of these methods and essentially originated from partitioning ambiguity between two decay chains and/or ordering ambiguity in each decay chain.

- *Limited use of the available experimental information.* The so called transverse variables evidently neglect the longitudinal information measured in the detector.

In light of all these various assumptions, it is certainly desirable to have a *universal* method which can be applied to *any* event topology using full available experimental informations. Additional requirement of inclusivity which treats jets and leptons on an equal footing can ensure free of any of the said combinatorial ambiguities. To the best of our knowledge, the only such method in the literature is the one proposed in ref. [1], where the $\sqrt{s}_{\rm min}$ variable was first introduced.

In spite of several unique advantages, the $\sqrt{s}_{\rm min}$ variable has not yet found wide application. The one major perceived drawback of $\sqrt{s}_{\rm min}$ is its sensitivity to initial state radiation (ISR) and/or multiple parton interactions (MPI) [1, 6, 41–43]. To see how this comes about, let us first review the formal definition of $\sqrt{s}_{\rm min}$.

1.2 Definition of $\sqrt{s}_{\rm min}$

Consider the most generic missing energy event topology. Each event contains some number n_{vis} of Standard Model (SM) particles, energies and momenta ($P^\mu \equiv (E, \vec{P})$) of which are in principle measured in the detector. In turn, the missing transverse momentum $\vec{\not{P}}_T$ can arise from a certain number n_{inv} of stable neutral particles which are *invisible* in the detector. In general, the set of invisible particles can be either SM neutrinos or may originate from BSM. The $\vec{\not{P}}_T$ measurement alone does not reveal the number of missing particles, nor how many of them are neutrinos and how many are BSM (dark matter) particles.

Given this very general setup, ref. [1] asked the following question: What is the *minimum* value $\sqrt{s}_{\rm min}$ of the parton-level Mandelstam invariant mass variable $\sqrt{s}$ which is

JHEP06(2011)041

consistent with the observed visible 4-momentum vector $P^\mu \equiv (E, \vec{P})$? As it turned out, the answer to this question is given by the universal formula [1]

$$\sqrt{s}_{\rm min}(\not{M}) \equiv \sqrt{E^2 - P_z^2} + \sqrt{\not{M}^2 + \not{P}_T^2}\,, \tag{1.1}$$

where the mass parameter $\not{M}$ is nothing but the total mass of all invisible particles in the event:

$$\not{M} \equiv \sum_{i=1}^{n_{inv}} m_i = \sum_{i=1}^{n_\chi} m_i\,, \tag{1.2}$$

and the second equality follows from the assumption of vanishing neutrino masses. The result (1.1) can be equivalently rewritten in a more symmetric form

$$\sqrt{s}_{\rm min}(\not{M}) = \sqrt{M^2 + P_T^2} + \sqrt{\not{M}^2 + \not{P}_T^2} \tag{1.3}$$

in terms of the total visible invariant mass M defined as

$$M^2 \equiv E^2 - P_x^2 - P_y^2 - P_z^2 \equiv E^2 - P_T^2 - P_z^2\,. \tag{1.4}$$

Notice that in spite of the complete arbitrariness of the invisible particle sector at this point, the definition of $\sqrt{s}_{\rm min}$ depends on a single unknown parameter $\not{M}$ - the *sum* of all the masses of the invisible particles in the event. For future reference, one should keep in mind that transverse momentum conservation at this point implies that

$$\vec{P}_T + \vec{\not{P}}_T = 0. \tag{1.5}$$

The main result from ref. [1] was that in the absence of ISR and MPI, the peak in the $\sqrt{s}_{\rm min}$ distribution nicely correlates with the mass threshold of the newly produced particles. This observation provides one generic relation between the total mass of the produced particles and the total mass $\not{M}$ of the invisible particles. Based on several SUSY examples involving fully hadronic signatures in symmetric as well as asymmetric topologies, ref. [1] showed that the accuracy of this measurement rivals the one achieved with the more traditional M_{T2} methods.

1.3 $\sqrt{s}_{\rm min}$ and the underlying event problem

At the same time, it was also recognized that effects from ISR and MPI severely jeopardize this measurement. The problem is that in the presence of the underlying events (UE),[1] the $\sqrt{s}_{\rm min}$ variable would be measuring *the total* energy of the full system, while for studying any new physics we are mostly interested in the energy of the hard scattering. The inclusion of the UE causes a drastic shift of the peak of the $\sqrt{s}_{\rm min}$ distribution to higher values, often by as much as a few TeV [1, 41, 42]. As a result, it appeared that unless effects from the underlying event could somehow be compensated for, the proposed measurement of the $\sqrt{s}_{\rm min}$ peak would be of no practical value.

The main purpose of this paper is to propose two fresh new approaches to dealing with the underlying event problem which has plagued the $\sqrt{s}_{\rm min}$ variable and prevented

[1] In this definition, the UE is everything else other than the hard scattering.

JHEP06(2011)041

its more widespread use in hadron collider physics applications. But before we discuss the two new ideas put forth in this paper, we first briefly mention the two existing proposals in the literature on how to deal with the underlying event problem.

First, it was recognized in ref. [1] that the contributions from the underlying event tend to be in the forward region, i.e. at large values of $|\eta|$. Correspondingly, by choosing a suitable cut $|\eta| < \eta_{\max}$, designed to eliminate contributions from the very forward regions, one could in principle restore the proper behavior of the $\sqrt{s}_{\min}$ distribution [1]. Unfortunately, there are no a priori guidelines on how to choose the appropriate value of $\eta_{\max}$, therefore this approach introduces an uncontrollable systematic error and has not been pursued further in the literature.

An alternative approach was proposed in refs. [41, 42], which pointed out that the ISR effects on $\sqrt{s}_{\min}$ are in principle calculable in QCD from first principles. The calculations presented in refs. [41, 42] could then be used to "unfold" the ISR effects and correct for the shift in the peak of the $\sqrt{s}_{\min}$ distribution. Unfortunately, in this analytical approach, the MPI effects would still be unaccounted for, and would have to be modeled and validated separately by some other means. While such an approach may eventually bear fruit at some point in the future, we shall not pursue it here.

We see that, for one reason or another, both of these strategies appear unsatisfactory. Therefore, here we shall pursue two different approaches. We shall propose two new variants of the $\sqrt{s}_{\min}$ variable, which we label $\sqrt{s}^{(reco)}_{\min}$ and $\sqrt{s}^{(sub)}_{\min}$ and define in sections 2 and 3, correspondingly. We illustrate the properties of these two variables with several examples in sections 4–6. These examples will show that both $\sqrt{s}^{(reco)}_{\min}$ and $\sqrt{s}^{(sub)}_{\min}$ are unharmed by the effects from the underlying event, thus resurrecting the original idea of ref. [1] to use the peak in the $\sqrt{s}_{\min}$ distribution as a first, quick, model-independent estimate of the new physics mass scale. In section 7 we compare the performance of $\sqrt{s}_{\min}$ against some other inclusive variables which are commonly used in hadron collider physics for the purpose of estimating the new physics mass scale. Section 8 is reserved for our main summary and conclusions.

2 Definition of the RECO level variable $\sqrt{s}^{(reco)}_{\min}$

In this first approach, we shall *not* modify the original definition of $\sqrt{s}_{\min}$ and will continue to use the usual equation (1.1) (or its equivalent (1.3)), preserving the desired universal, global and inclusive character of the $\sqrt{s}_{\min}$ variable. We shall rather concentrate on the question, how should one calculate the observable quantities E, $\vec{P}$ and $\not{P}_T$ entering these defining equations.

The previous $\sqrt{s}_{\min}$ studies [1, 41, 42] used calorimeter-based measurements of the total visible energy $E_{(cal)}$ and momentum $\vec{P}_{(cal)}$. Thus one can construct the "calorimeter-based" $\sqrt{s}_{\min}$ variable as

$$\sqrt{s}^{(cal)}_{\min}(\not{M}) \equiv \sqrt{E^2_{(cal)} - P^2_{z(cal)}} + \sqrt{\not{M}^2 + \not{P}^2_{T(cal)}} \,. \tag{2.1}$$

This was precisely the quantity which was studied in [1, 41, 42] and shown to exhibit extreme sensitivity to the physics of the underlying event.

JHEP06(2011)041

Here we propose to evaluate the visible quantities E and $\vec{P}$ at the RECO level, i.e. in terms of the reconstructed objects, namely jets, muons, electrons and photons.[2] To be precise, let there be N_{obj} reconstructed objects in the event, with energies E_i and 3-momenta $\vec{P}_i$, $i = 1, 2, \ldots, N_{obj}$, correspondingly. Then in place of calorimeter based measurements, let us instead identify

$$E \equiv E_{(reco)} \equiv \sum_{i=1}^{N_{obj}} E_i \,, \tag{2.2}$$

$$\vec{P} \equiv \vec{P}_{(reco)} \equiv \sum_{i=1}^{N_{obj}} \vec{P}_i \,, \tag{2.3}$$

$$\vec{\not{P}}_T \equiv \vec{\not{P}}_{T(reco)} = -\vec{P}_{T(reco)} \,, \tag{2.4}$$

and correspondingly define a "RECO-level" $\sqrt{s}_{\rm min}$ variable as

$$\sqrt{s}^{(reco)}_{\rm min}(\not{M}) \equiv \sqrt{E^2_{(reco)} - P^2_{z(reco)}} + \sqrt{\not{M}^2 + \not{P}^2_{T(reco)}} \,, \tag{2.5}$$

which can also be rewritten in analogy to (1.3) as

$$\sqrt{s}^{(reco)}_{\rm min}(\not{M}) \equiv \sqrt{M^2_{(reco)} + P^2_{T(reco)}} + \sqrt{\not{M}^2 + \not{P}^2_{T(reco)}} \,, \tag{2.6}$$

where $\not{P}_{T(reco)}$ and $P_{T(reco)}$ are related as in eq. (2.4) and the RECO-level total visible mass $M_{(reco)}$ is defined by

$$M^2_{(reco)} \equiv E^2_{(reco)} - \vec{P}^2_{(reco)} \,. \tag{2.7}$$

What are the benefits from the new RECO-level $\sqrt{s}_{\rm min}$ definitions (2.5), (2.6) in comparison to the old calorimeter-based $\sqrt{s}_{\rm min}$ definition in (2.1)? In order to understand the basic idea, it is worth comparing the calorimeter-based missing transverse momentum $\not{P}_T$ (which in the literature is commonly referred to as "missing transverse energy" $\not{E}_T$) and the analogous RECO-level variable $\not{H}_T$, the "missing H_T". The $\vec{\not{H}}_T$ vector is defined as the negative of the vector sum of the transverse momenta of all reconstructed objects in the event:

$$\vec{\not{H}}_T \equiv -\sum_{i=1}^{N_{obj}} \vec{P}_{Ti} \,. \tag{2.8}$$

Then it is clear that in terms of our notation here, $\not{H}_T$ is nothing but $\not{P}_{T(reco)}$.

It is known that $\not{H}_T$ performs better than $\not{E}_T$ [44]. First, $\not{H}_T$ is less affected by a number of adverse instrumental factors such as: electronic noise, faulty calorimeter cells, pile-up, etc. These effects tend to populate the calorimeter uniformly with unclustered energy, which will later fail the basic quality cuts during object reconstruction. In contrast, the *true* missing momentum is dominated by clustered energy, which will be successfully captured during reconstruction. Another advantage of $\not{H}_T$ is that one can easily apply the known jet energy corrections to account for the nonlinear detector response. For both of these reasons, CMS is now using $\not{H}_T$ at both the trigger level and offline [44].

[2] This possibility was briefly alluded to in [1], but not pursued in any detail.

JHEP06(2011)041

Now realize that $\sqrt{\hat{s}}_{\rm min}^{(cal)}$ is analogous to the calorimeter-based $\not{E}_T$, while our new variable $\sqrt{\hat{s}}_{\rm min}^{(reco)}$ is analogous to the RECO-level $\not{H}_T$. Thus we may already expect that $\sqrt{\hat{s}}_{\rm min}^{(reco)}$ will inherit the advantages of $\not{H}_T$ and will be better suited for determining the new physics mass scale than the calorimeter-based quantity $\sqrt{\hat{s}}_{\rm min}^{(cal)}$. This expectation is confirmed in the explicit examples studied below in sections 4 and 5. Apart from the already mentioned instrumental issues, the most important advantage of $\sqrt{\hat{s}}_{\rm min}^{(reco)}$ from the physics point of view is that it is much less sensitive to the effects from the underlying event, which had doomed its calorimeter-based $\sqrt{\hat{s}}_{\rm min}^{(cal)}$ cousin.

Strictly speaking, the idea of $\sqrt{\hat{s}}_{\rm min}^{(reco)}$ does not solve the underlying event problem completely and as a matter of principle. Every now and then the underlying event will still produce a well-defined jet, which will have to be included in the calculation of $\sqrt{\hat{s}}_{\rm min}^{(reco)}$. Because of this effect, we cannot any more guarantee that $\sqrt{\hat{s}}_{\rm min}^{(reco)}$ provides a lower bound on the true value $\sqrt{\hat{s}}_{true}$ of the center-of-mass energy of the hard scattering — the additional jets formed out of ISR, pile-up, and so on, will sometimes cause $\sqrt{\hat{s}}_{\rm min}^{(reco)}$ to exceed $\sqrt{\hat{s}}_{true}$. Nevertheless we find that this effect modifies only the shape of the $\sqrt{\hat{s}}_{\rm min}^{(reco)}$ distribution, but leaves the location of its peak largely intact. To the extent that one is mostly interested in the peak location, $\sqrt{\hat{s}}_{\rm min}^{(reco)}$ should already be good enough for all practical purposes.

In the rest of this section, we would like to point out some interesting observations relating the present variable with other inclusive variables in the literature. Comparison with the visible mass M_{vis} [45], the missing energy, $\not{E}_T$, the visible transverse energy E_T and the effective mass has already been discussed in refs. [1, 41, 42], and other inclusive variables such as $\vec{\not{H}}_T$ and $\not{H}_T$, M_{Tgen}, M_{TTgen} will be discussed in section 7. Here we concentrate on two other variables, e.g. cluster variables and m_T^{true}.

It turns out that the $\sqrt{\hat{s}}_{\rm min}$ variable has been already proved to be very useful in literature in the past. Some of global variables proposed for a signature with more than one missing particle are in fact the $\sqrt{\hat{s}}_{\rm min}$ variable hidden in their analytic expressions, although they are not derived by any systematic minimization of $\sqrt{\hat{s}}$ and thus blur the physical insight of these variables. Now we understand they are particular examples in the application of $\sqrt{\hat{s}}_{\rm min}$, which can be derived from the first principle. In particular, some of these variables are proposed in search for the Higgs physics. For instance, the cluster transverse mass is defined as

$$M_{T,WW}^2 = \left(\sqrt{P_{T,jje}^2 + M_{jje}^2} + \not{E}_T\right)^2 - \left(\vec{P}_{T,jje} + \vec{\not{P}}_T\right)^2, \tag{2.9}$$

and

$$M_{C,WW}^2 = \left(\sqrt{P_{T,\ell\ell}^2 + M_{\ell\ell}^2} + \not{E}_T\right)^2 - \left(\vec{P}_{T,\ell\ell} + \vec{\not{P}}_T\right)^2, \tag{2.10}$$

for $H \to W^+W^- \to \ell + jj + \not{E}_T$ and $H \to W^+W^- \to \ell^+\ell^- + \not{E}_T$, respectively [46]. This is precisely the $\sqrt{\hat{s}}_{\rm min}$ variable being discussed in the paper. The effective transverse mass,

$$M_{eff\ T}^2 = \left(E_{\ell^+T} + E_{\ell^-T} + \not{E}_T\right)^2 - \left(\vec{P}_{\ell^+T} + \vec{P}_{\ell^-T} + \vec{\not{P}}_T\right)^2 \tag{2.11}$$

$$= \left(E_{\ell^+T} + E_{\ell^-T} + \not{E}_T\right)^2, \tag{2.12}$$

JHEP06(2011)041

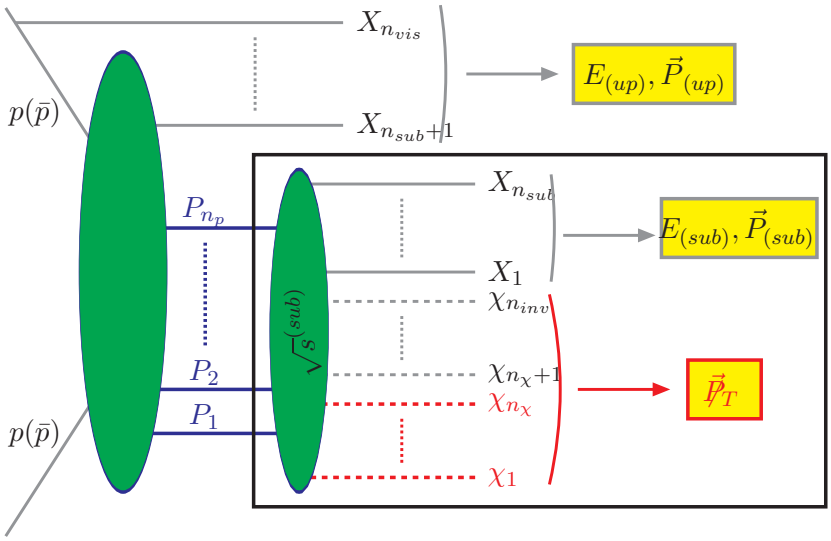

Figure 1. An event topology exhibiting a well defined subsystem (delineated by the black rectangle) with total invariant mass $\sqrt{s}^{(sub)}$. There are n_{sub} visible particles X_i, $i = 1, 2, \ldots, n_{sub}$, originating from within the subsystem, while the remaining $n_{vis} - n_{sub}$ visible particles $X_{n_{sub}+1}, \ldots, X_{n_{vis}}$ are created upstream, outside the subsystem. The subsystem results from the production and decays of a certain number of parent particles P_j, $j = 1, 2, \ldots, n_p$, (some of) which may decay semi-invisibly. All invisible particles $\chi_1, \ldots, \chi_{n_{inv}}$ are then assumed to originate from within the subsystem.

just looks like another version of $\sqrt{s}_{\min}$, projecting each momentum onto transverse plane first before combining visible sectors [46]. This is recently reexamined as m_T^{true} in ref. [47], improving the discovery potential of the Higgs particle in the dilepton channel (see also [45] for comparison with the visible mass.).

In the case of $H \to ZZ \to \ell^+\ell^- + \nu\bar{\nu}$, the cluster variable is defined as

$$M_{T,ZZ}^2 = \left(E_{T,Z_1} + E_{T,Z_2}\right)^2 - \left(\vec{P}_{T,Z_1} + \vec{P}_{T,Z_2}\right)^2 \tag{2.13}$$

$$= \left(\sqrt{P_{T,\ell\ell}^2 + M_Z^2} + \sqrt{\not{E}_T^2 + M_Z^2}\right)^2 - \left(\vec{P}_{T,\ell\ell} + \vec{\not{P}}_T\right)^2, \tag{2.14}$$

and it is another application of $\sqrt{s}_{\min}$ variable.

3 Definition of the subsystem variable $\sqrt{s}_{\min}^{(sub)}$

In this section we propose an alternative modification of the original $\sqrt{s}_{\min}$ variable, which in principle solves the underlying event problem completely. The downside of this approach is that it is not as general and universal as the one discussed in the previous section, and can be applied only in cases where one can unambiguously identify a subsystem of the original event topology which is untouched by the underlying event. The basic idea is schematically illustrated in figure 1 exhibiting a well defined subsystem (delineated by

JHEP06(2011)041

the black rectangle). Visible particle X_i have been divided into two groups: (a) n_{sub} visible particles within the subsystem having total energy-momentum as $E_{(sub)}$ and $\vec{P}_{(sub)}$ correspondingly. The subsystem particles are chosen so that to guarantee that they could not have come from the ISR or UE. (b) The remaining visible particles including those from ISR are upstream objects (outside the subsystem) having total energy-momentum as $E_{(up)}$ and $\vec{P}_{(up)}$. We also assume that all invisible particles originate only from within the subsystem.

At this point the reader may be wondering what are the guiding principles for categorizing a given visible particle X_i as a subsystem or an upstream particle. Since our goal is to identify a subsystem which is shielded from the effects of the underlying event, the safest way to do the partition of the visible particles is to require that all QCD jets belong to the upstream particles, while the subsystem particles consist of objects which are unlikely to come from the underlying event, such as isolated electrons, photons and muons (and possibly identified τ-jets and, to a lesser extent, tagged b-jets). One may try to isolate ISR jets from jets coming from a heavy particle decay, and thus increase the scope of subsystem $\sqrt{s}_{\min}$ with much wider application. However sorting out the combinatorics of an event is a very difficult task although several approaches have been suggested [41, 42, 48–60]. In this paper we are interested in a correlation between mass of the intermediate particle and $\sqrt{s}_{\min}^{(sub)}$, for a given topology.

With those preliminaries, we are now ready to ask the usual $\sqrt{s}_{\min}$ question: Given the measured values of $E_{(up)}$, $E_{(sub)}$, $\vec{P}_{(up)}$ and $\vec{P}_{(sub)}$, what is the minimum value $\sqrt{s}_{\min}^{(sub)}$ of the *subsystem* Mandelstam invariant mass variable $\sqrt{s}^{(sub)}$, which is consistent with those measurements? Proceeding as in [1], once again we find a very simple universal answer, which can be equivalently written in several different ways as follows:

$$\sqrt{s}_{\min}^{(sub)}(\not{M}) = \left\{ \left(\sqrt{E_{(sub)}^2 - P_{z(sub)}^2} + \sqrt{\not{M}^2 + \not{P}_T^2} \right)^2 - P_{T(up)}^2 \right\}^{\frac{1}{2}} \tag{3.1}$$

$$= \left\{ \left(\sqrt{M_{(sub)}^2 + P_{T(sub)}^2} + \sqrt{\not{M}^2 + \not{P}_T^2} \right)^2 - P_{T(up)}^2 \right\}^{\frac{1}{2}} \tag{3.2}$$

$$= \left\{ \left(\sqrt{M_{(sub)}^2 + P_{T(sub)}^2} + \sqrt{\not{M}^2 + \not{P}_T^2} \right)^2 - (\vec{P}_{T(sub)} + \vec{\not{P}}_T)^2 \right\}^{\frac{1}{2}} \tag{3.3}$$

$$= ||p_{T(sub)} + \not{p}_T|| \,, \tag{3.4}$$

where in the last line we have introduced the Lorentz 1+2 vectors

$$p_{T(sub)} \equiv \left(\sqrt{M_{(sub)}^2 + P_{T(sub)}^2} \,,\, \vec{P}_{T(sub)} \right) ; \tag{3.5}$$

$$\not{p}_T \equiv \left(\sqrt{\not{M}^2 + \not{P}_T^2} \,,\, \vec{\not{P}}_T \right) . \tag{3.6}$$

As usual, the length of a 1+2 vector is computed as $||p|| = \sqrt{p \cdot p} = \sqrt{p_0^2 - p_1^2 - p_2^2}$.

Since our goal is to identify a subsystem which is shielded from the effects of the underlying event, the safest way to do the partition of the visible particles is simply requiring

JHEP06(2011)041

that all QCD jets belong to the upstream particles, while the subsystem particles consist of reconstructed objects which are unlikely to come from the underlying event, such as isolated electrons, photons and muons (and possibly identified τ-jets and, to a lesser extent, tagged b-jets).

This concept is most useful when the subsystem results from the production and decays of a certain number of heavy parent particles. Then the total combined parent mass can approximately be measured by the location of the peak of the $\sqrt{s}_{\min}^{(sub)}(\not{M})$ distribution. Subsystem analysis, even though restricted, can carry additional information along with full reco level study.[3]

4 SM example: dilepton events from $t\bar{t}$ production

In this and the next two sections we illustrate the properties of the new variables $\sqrt{s}_{\min}^{(reco)}$ and $\sqrt{s}_{\min}^{(sub)}$ with some specific examples. In this section we discuss an example taken from the Standard Model, which is guaranteed to be available for early studies at the LHC. We consider dilepton events from $t\bar{t}$ pair production, where both W's decay leptonically. In this event topology, there are two missing particles (two neutrinos). Therefore, these events very closely resemble the typical SUSY-like events, in which there are two missing dark matter particles. In the next two sections, we shall also consider some SUSY examples. In all cases, we perform detailed event simulation, including the effects from the underlying event and detector resolution.

4.1 Event simulation details

Events are generated with PYTHIA [61] (using its default model of the underlying event) at an LHC of 14 TeV, and then reconstructed with the PGS detector simulation package [62]. We have made certain modifications in the publicly available version of PGS to better match it to the CMS detector. For example, we take the hadronic calorimeter resolution to be [63]

$$\frac{\sigma}{E} = \frac{120\%}{\sqrt{E}}\,, \tag{4.1}$$

while the electromagnetic calorimeter resolution is [63]

$$\left(\frac{\sigma}{E}\right)^2 = \left(\frac{S}{\sqrt{E}}\right)^2 + \left(\frac{N}{E}\right)^2 + C^2\,, \tag{4.2}$$

where the energy E is measured in GeV, $S = 3.63\%$ is the stochastic term, $N = 0.124$ is the noise and $C = 0.26\%$ is the constant term. Muons are reconstructed within $|\eta| < 2.4$,

[3] Note that the typical hadron collider signatures of the most popular new physics models (supersymmetry, extra dimensions, Little Higgs, etc.) are precisely of the form exhibited in figure 1. One typically considers production of colored particles (squarks, gluinos, KK-quarks, etc.) whose cross-sections dominate. In turn, these colored particles shed their color charge by emitting jets and decaying to lighter, uncolored particles in an electroweak sector. The decays of the latter often involve electromagnetic objects, which could be targeted for selection in the subsystem. The $\sqrt{s}_{\min}^{(sub)}$ variable would then be the perfect tool for studying the mass scales in the electroweak sector (in the context of supersymmetry, for example, the electroweak sector is composed of the charginos, neutralinos and sleptons).

JHEP06(2011)041

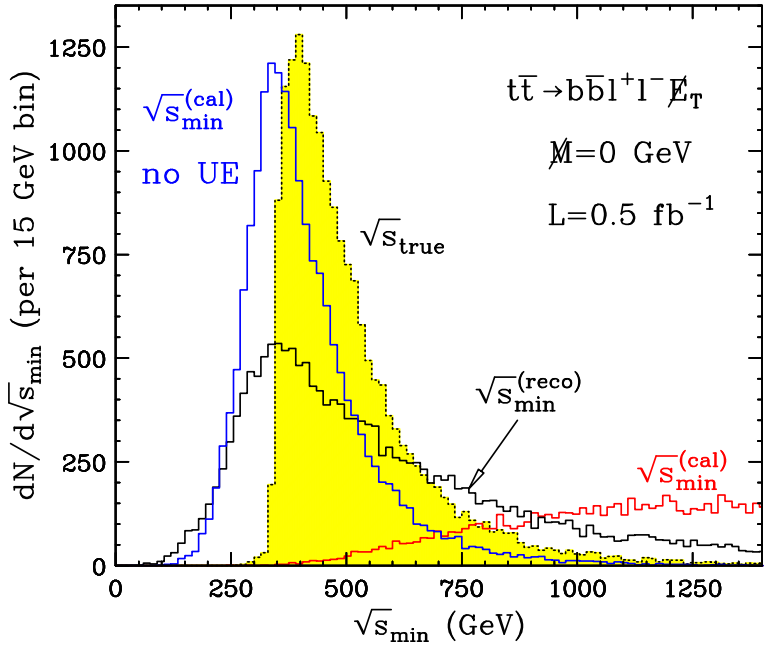

Figure 2. Distributions of various $\sqrt{s}_{\rm min}$ quantities discussed in the text, for the dilepton $t\bar{t}$ sample at the LHC with 14 TeV CM energy and 0.5 fb^{-1} of data. The dotted (yellow-shaded) histogram gives the true $\sqrt{s}$ distribution of the $t\bar{t}$ pair. The blue histogram is the distribution of the calorimeter-based $\sqrt{s}_{\rm min}^{(cal)}$ variable in the ideal case when all effects from the underlying event are turned off. The red histogram shows the corresponding result for $\sqrt{s}_{\rm min}^{(cal)}$ in the presence of the underlying event. The black histogram is the distribution of the $\sqrt{s}_{\rm min}^{(reco)}$ variable introduced in section 2. All $\sqrt{s}_{\rm min}$ distributions are shown for $\not{M} = 0$.

and we use the muon global reconstruction efficiency quoted in [63]. We use default p_T cuts on the reconstructed objects as follows: 3 GeV for muons, 10 GeV for electrons and photons, and 15 GeV for jets.

For the $t\bar{t}$ example presented in this section, we use the approximate next-to-next-to-leading order $t\bar{t}$ cross-section of $\sigma_{t\bar{t}} = 873$ pb at a top mass of $m_t = 175$ GeV [64]. For the SUSY examples in the next two sections we use leading order cross-sections.

Since our examples are meant for illustration purposes only, we do not include any backgrounds to the processes being considered, nor do we require any specific triggers. A detailed study of the dilepton $t\bar{t}$ signature including all those effects will appear elsewhere [65].

4.2 $\sqrt{s}_{\rm min}^{(reco)}$ variable

We first consider SUSY-like missing energy events arising from $t\bar{t}$ production, where each W-boson is forced to decay leptonically (to an electron or a muon). We do not impose any trigger or offline requirements, and simply plot directly the output from PGS. We show various $\sqrt{s}$ quantities of interest in figure 2, setting $\not{M} = 0$, since in this case the missing particles are neutrinos and are massless. The dotted (yellow-shaded) histogram represents

JHEP06(2011)041

Event type	PYTHIA parton level		after PGS simulation	
	$\sqrt{s}_{true}$	$\sqrt{s}^{(cal)}_{\rm min}$	$\sqrt{s}^{(cal)}_{\rm min}$	$\sqrt{s}^{(reco)}_{\rm min}$
$t\bar{t}$ event in figure 3	427	1110	1179	363
$t\bar{t}$ event in figure 4	638	2596	2761	736
SUSY event in figure 11	1954	3539	3509	2085

Table 1. Selected $\sqrt{s}$ quantities (in GeV) for the events shown in figures 3, 4 and 11. The second column shows the true invariant mass $\sqrt{s}_{true}$ of the parent system: top quark pair in case of figures 3 and 4, or gluino pair in case of figure 11. The third column shows the value of the $\sqrt{s}^{(cal)}_{\rm min}$ variable (2.1) calculated at the parton level, without any PGS detector simulation, but with the full detector acceptance cut of $|\eta| < 4.1$. The fourth column lists the value of $\sqrt{s}^{(cal)}_{\rm min}$ obtained after PGS detector simulation, while the last column shows the value of the $\sqrt{s}^{(reco)}_{\rm min}$ variable defined in (2.5).

the true $\sqrt{s}$ distribution of the $t\bar{t}$ pair. It quickly rises at the $t\bar{t}$ mass threshold

$$M_p \equiv 2m_t = 350 \text{ GeV} \tag{4.3}$$

and then eventually falls off at large $\sqrt{s}$ due to the parton density function suppression. Because the top quarks are typically produced with some boost, the $\sqrt{s}_{true}$ distribution in figure 2 peaks a little bit above threshold. It is clear that if one could directly measure the $\sqrt{s}_{true}$ distribution, or at least its onset, the $t\bar{t}$ mass scale will be easily revealed. Unfortunately, the escaping neutrinos make such a measurement impossible, unless one is willing to make additional model-dependent assumptions.[4]

Our first main result is nicely summarized in figure 2, which shows a total of 4 distributions, 3 of which are either unphysical (the blue histogram of $\sqrt{s}^{(cal)}_{\rm min}$ *in the absence* of the UE), unobservable (the yellow-shaded histogram of $\sqrt{s}_{true}$), or useless (the red histogram of $\sqrt{s}^{(cal)}_{\rm min}$ *in the presence* of the UE). The only distribution in figure 2 which is physical, observable and useful at the same time, is the distribution of $\sqrt{s}^{(reco)}_{\rm min}$ (solid black histogram). This variable in fact retains the peak of the distribution at the much desired physical threshold:

$$\left(\sqrt{s}^{(reco)}_{\rm min}\right)_{peak} \approx M_p\,, \tag{4.4}$$

Let us now see how the calculation of $\sqrt{s}^{(reco)}_{\rm min}$ is affected by the UE. Since object reconstruction is done with the help of minimum *transverse* cuts (for clustering and object id), the relevant calorimeter plots are the maps on the right side in figure 3. We see that the large forward energy deposits which were causing the large shift in $\sqrt{s}^{(cal)}_{\rm min}$ are

[4]For example, one can use the known values of the neutrino, W and top masses to solve for the neutrino kinematics (up to discrete ambiguities). However, this method assumes that the full mass spectrum is already known, and furthermore, uses the knowledge of the top decay topology to perfectly solve the combinatorics problem discussed in the Introduction. As an example, consider a case where the lepton is produced first and the b-quark second, i.e. when the top first decays to a lepton and a leptoquark, which in turn decays to a neutrino and a b-quark. The kinematic method would then be using the wrong on-shell conditions. The advantage of the $\sqrt{s}_{\rm min}$ approach is that it is fully inclusive and does not make any reference to the actual decay topology.

JHEP06(2011)041

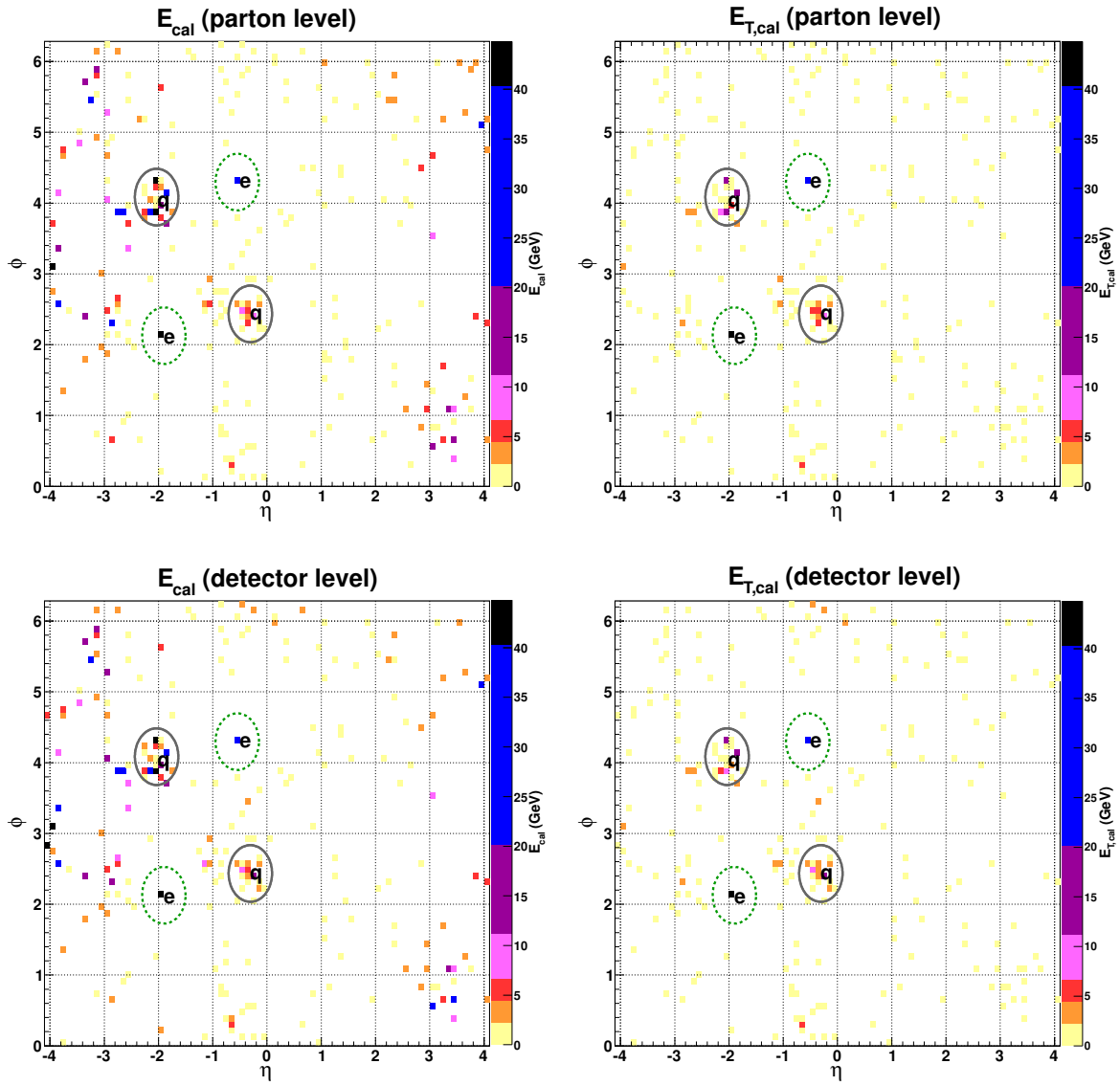

Figure 3. PGS calorimeter map of the energy deposits, as a function of pseudorapidity η and azimuthal angle ϕ, for a dilepton $t\bar{t}$ event with only two reconstructed jets. At the parton level, this particular event has two b-quarks and two electrons. The location of a b-quark (electron, muon) is marked with the letter "q" ("e", "μ"). A grey circle delineates (the cone of) a reconstructed jet, while a green dotted circle denotes a reconstructed lepton. In the upper two plots the calorimeter is filled at the parton level directly from PYTHIA, while the lower two plots contain results after PGS simulation. The left plots show absolute energy deposits E_α, while in the right plots the energy in each tower is shown projected on the transverse plane as $E_\alpha \cos\theta_\alpha$.

not incorporated into any reconstructed objects, and thus do not contribute to the $\sqrt{s}_{\rm min}^{(reco)}$ calculation at all. In effect, the RECO-level prescription for calculating $\sqrt{s}_{\rm min}$ is leaving out precisely the unwanted contributions from the UE, while keeping the relevant contributions from the hard scattering. As seen from table 1, the calculated value of $\sqrt{s}_{\rm min}^{(reco)}$ for that

JHEP06(2011)041

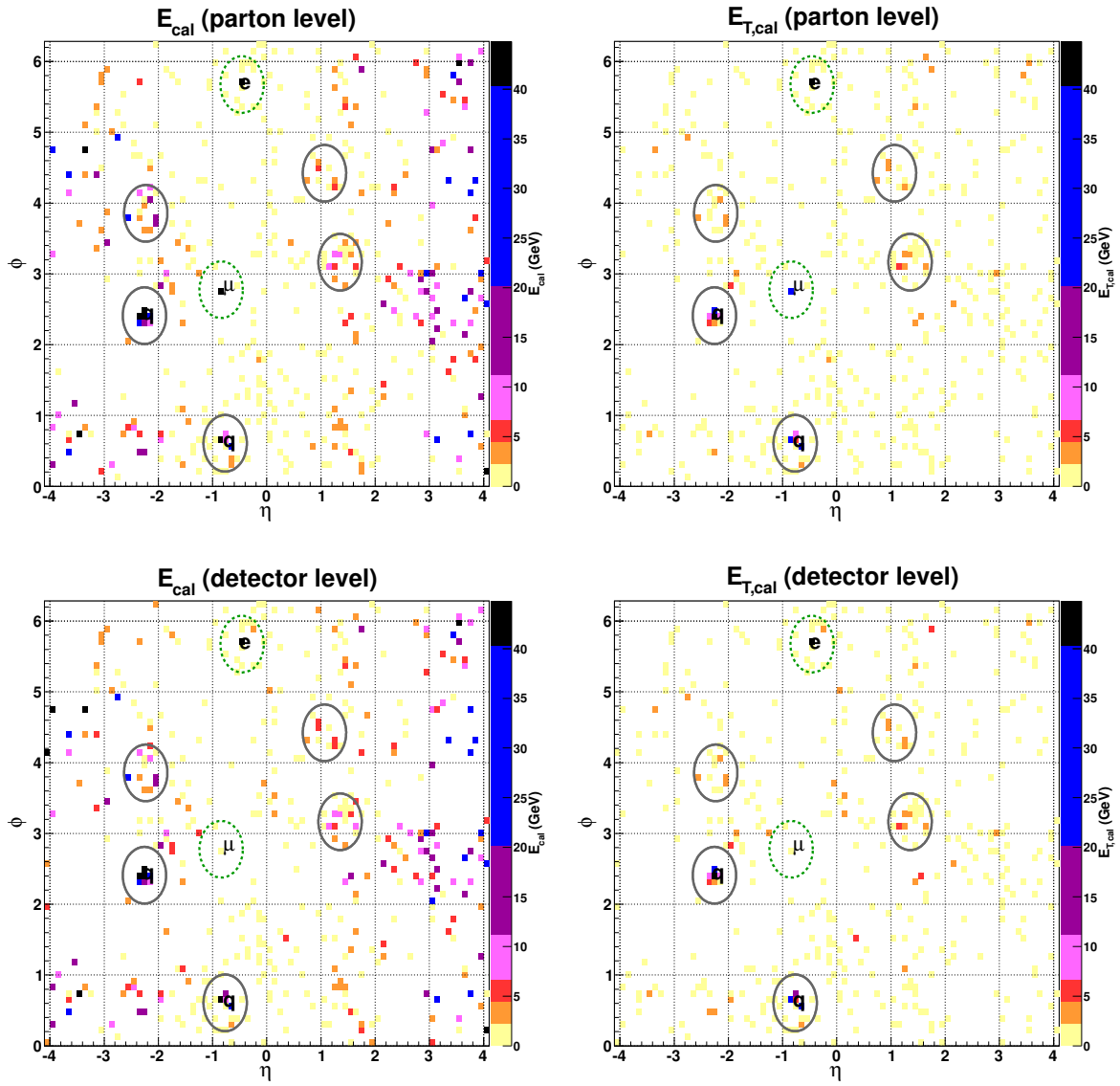

Figure 4. The same as figure 3, but for an event with three additional reconstructed jets.

event is 363 GeV, which is indeed very close to the $t\bar{t}$ threshold. It is also smaller than the true $\sqrt{s}$ value of 427 GeV in that event, which is to be expected, since by design $\sqrt{s}_{\rm min} \leq \sqrt{s}$, and this event does not have any extra ISR jets to spoil this relation.

It is instructive to consider another, more complex $t\bar{t}$ dilepton event, such as the one shown in figure 4. The corresponding calculated values for $\sqrt{s}_{\rm min}^{(cal)}$ and $\sqrt{s}_{\rm min}^{(reco)}$ are shown in the second row of table 1. As seen in figure 4, this event has additional jets and a lot more UE activity. As a result, the calculated value of $\sqrt{s}_{\rm min}^{(cal)}$ is shifted by almost 2 TeV from the nominal $\sqrt{s}_{true}$ value. Nevertheless, the RECO-level prescription nicely compensates for this effect, and the calculated $\sqrt{s}_{\rm min}^{(reco)}$ value is only 736 GeV, which is within 100 GeV of the nominal $\sqrt{s}_{true} = 638$ GeV. Notice that in this example we end up with a situation

JHEP06(2011)041

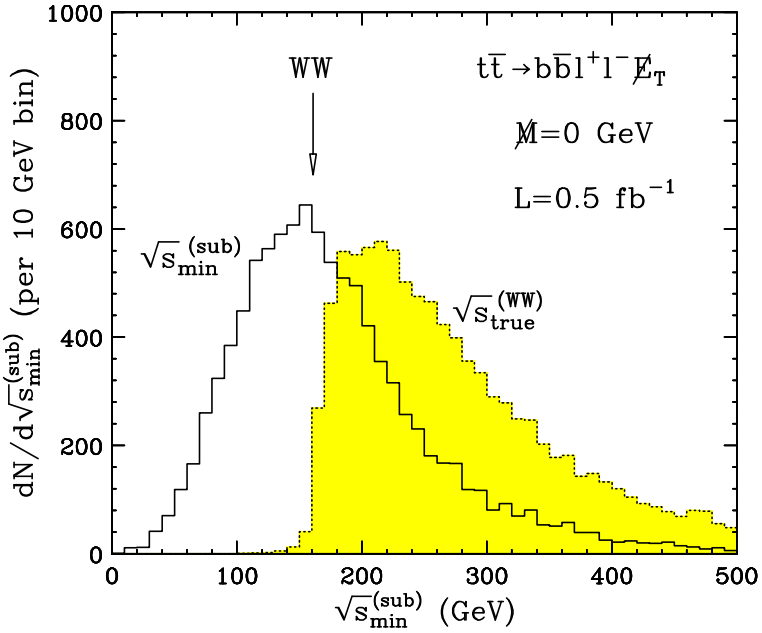

Figure 5. The same as figure 2, but for the dilepton subsystem in dilepton $t\bar{t}$ events with two reconstructed leptons in PGS. The dotted (yellow-shaded) histogram gives the true $\sqrt{s}$ distribution of the W^+W^- pair in those events. The black histogram shows the distribution of the (leptonic) subsystem variable $\sqrt{s}_{\rm min}^{(sub)}$ defined in section 3. In this case, the subsystem is defined by the two isolated leptons, while all jets are treated as upstream particles. The vertical arrow marks the W^+W^- mass threshold.

where $\sqrt{s}_{\rm min}^{(reco)} > \sqrt{s}_{true}$. Figure 2 indicates that this happens quite often — the tail of the $\sqrt{s}_{\rm min}^{(reco)}$ distribution is more populated than the (yellow-shaded) $\sqrt{s}_{true}$ distribution. This should be no cause for concern. First of all, we are only interested in the *peak* of the $\sqrt{s}_{\rm min}^{(reco)}$ distribution, and we do not need to make any comparisons between $\sqrt{s}_{\rm min}^{(reco)}$ and $\sqrt{s}_{true}$. Second, any such comparison would be meaningless, since the value of $\sqrt{s}_{true}$ is a priori unknown, and unobservable.

4.3 $\sqrt{s}_{\rm min}^{(sub)}$ variable

Before concluding this section, we shall use the $t\bar{t}$ example to also illustrate the idea of the subsystem $\sqrt{s}_{\rm min}^{(sub)}$ variable developed in section 3. Dilepton $t\bar{t}$ events are a perfect testing ground for this idea, since the WW subsystem decays leptonically, without any jet activity. We therefore define the subsystem as the two hard isolated leptons resulting from the decays of the W-bosons. Correspondingly, we require two reconstructed leptons (electrons or muons) at the PGS level,[5] and plot the distribution of the leptonic subsystem $\sqrt{s}_{\rm min}^{(sub)}$ variable in figure 5. As before, the dotted (yellow-shaded) histogram represents the true $\sqrt{s}$ distribution of the W^+W^- pair. As expected, it quickly rises at the WW threshold (denoted by the vertical arrow), then falls off at large $\sqrt{s}$. Since the $\sqrt{s}_{true}^{(WW)}$ distribution is

[5]The selection efficiency for the two leptons is on the order of 60%, which explains the different normalization of the distributions in figures 2 and 5.

JHEP06(2011)041

unobservable, the best we can do is to study the corresponding $\sqrt{s}_{\min}^{(sub)}$ distribution shown with the solid black histogram. In this subsystem example, all UE activity is lumped together with the upstream b-jets from the top quarks decays, and thus has no bearing on the properties of the leptonic $\sqrt{s}_{\min}^{(sub)}$. In particular, we find that the value of $\sqrt{s}_{\min}^{(sub)}$ is always smaller than the true $\sqrt{s}_{true}^{(WW)}$. More importantly, figure 5 demonstrates that the peak in the $\sqrt{s}_{\min}^{(sub)}$ distribution is found precisely at the mass threshold of the particles (in this case the two W bosons) which initiated the subsystem. Therefore, in analogy to (4.4) we can also write

$$\left(\sqrt{s}_{\min}^{(sub)}\right)_{peak} \approx M_p^{(sub)}\,, \tag{4.5}$$

where $M_p^{(sub)}$ is the combined mass of all the parents initiating the subsystem. Figure 5 shows that in the $t\bar{t}$ example just considered, this relation holds to a very high degree of accuracy.

This example should not leave the reader with the impression that hadronic jets are never allowed to be part of the subsystem. On the contrary — the subsystem may very well include reconstructed jets as well. The $t\bar{t}$ case considered here in fact provides a perfect example to illustrate the idea.

Let us reconsider the $t\bar{t}$ dilepton sample, and redefine the subsystem so that we now target the two *top quarks* as the parents initiating the subsystem. Correspondingly, in addition to the two leptons, let us allow the subsystem to include two jets, presumably coming from the two top quark decays. Unfortunately, in doing so, we must face a variant of the partitioning[6] combinatorial problem discussed in the introduction: as seen in figure 6, the typical jet multiplicity in the events is relatively high, and we must therefore specify the exact procedure how to select the two jets which would enter the subsystem. We shall consider three different approaches.

- *B-tagging.* We can use the fact that the jets from top quark decay are b-jets, while the jets from ISR are typically light flavor jets. Therefore, by requiring exactly two b-tags, and including only the two b-tagged jets as part of the subsystem, we can significantly increase the probability of selecting the correct jets. Of course, ISR will sometimes also contribute b-tagged jets from gluon splitting, but that happens rather rarely and the corresponding contribution can be suppressed by a further invariant mass cut on the two b-jets. The resulting $\sqrt{s}_{\min}^{(sub)}$ distribution for the subsystem of 2 leptons and 2 b-tagged jets is shown in figure 7 with the black histogram. We see that, as expected, the distribution peaks at the $t\bar{t}$ threshold and this time provides a measurement of the top quark mass:

  $$\left(\sqrt{s}_{\min}^{(sub)}\right)_{peak} \approx M_p^{(sub)} = 2m_t = 350\ \text{GeV}\,. \tag{4.6}$$

  The disadvantage of this method is the loss in statistics: compare the normalization of the black histogram in figure 7 after applying the two b-tags, to the dotted (yellow-shaded) distribution of the true $t\bar{t}$ distribution in the selected inclusive dilepton sample (without b-tags).

[6] By construction, the $\sqrt{s}_{\min}$ and $\sqrt{s}_{\min}^{(sub)}$ variables never have to face the *ordering* combinatorial problem.

JHEP06(2011)041

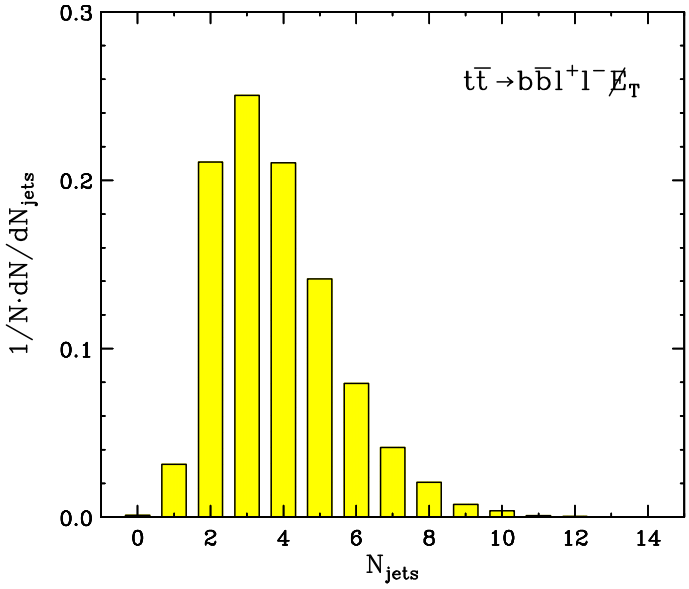

Figure 6. Unit-normalized distribution of jet multiplicity in dilepton $t\bar{t}$ events.

- *Selection by jet p_T.* Here one can use the fact that the jets from top decays are on average harder than the jets from ISR (the default p_T cut adopted by PGS is 15 GeV for jets). Correspondingly, by choosing the two highest p_T jets (regardless of b-tagging), one also increases the probability to select the correct jet pair. The corresponding distribution is shown in figure 7 with the blue histogram, and is also seen to peak at the $t\bar{t}$ threshold. An important advantage of this method is that one does not have to pay the price of reduced statistics due to the two additional b-tags.

- *No selection.* The most conservative approach would be to apply no selection criteria on the jets, and include all reconstructed jets in the subsystem. Then the subsystem $\sqrt{s}_{\rm min}^{(sub)}$ variable essentially reverts back to the RECO-level inclusive variable $\sqrt{s}_{\rm min}^{(reco)}$ already discussed in the previous subsection. Not surprisingly, we find the peak of its distribution (red histogram in figure 7) near the $t\bar{t}$ threshold as well.

All three of these examples show that jets can also be usefully incorporated into the subsystem. The only question is whether one can find a reliable way of preferentially selecting jets which are more likely to originate from within the intended subsystem, as opposed to from the outside. As we see in figure 7, in the $t\bar{t}$ case this is quite possible, although in general it may be difficult in other settings, like the SUSY examples discussed in the next section.

5 An exclusive SUSY example: multijet events from gluino production

Since $\sqrt{s}_{\rm min}$ is a fully inclusive variable, arguably its biggest advantage is that it can be applied to purely jetty events with large jet multiplicities, where no other method on the market would seem to work. In order to simulate such a challenging case, we consider

JHEP06(2011)041

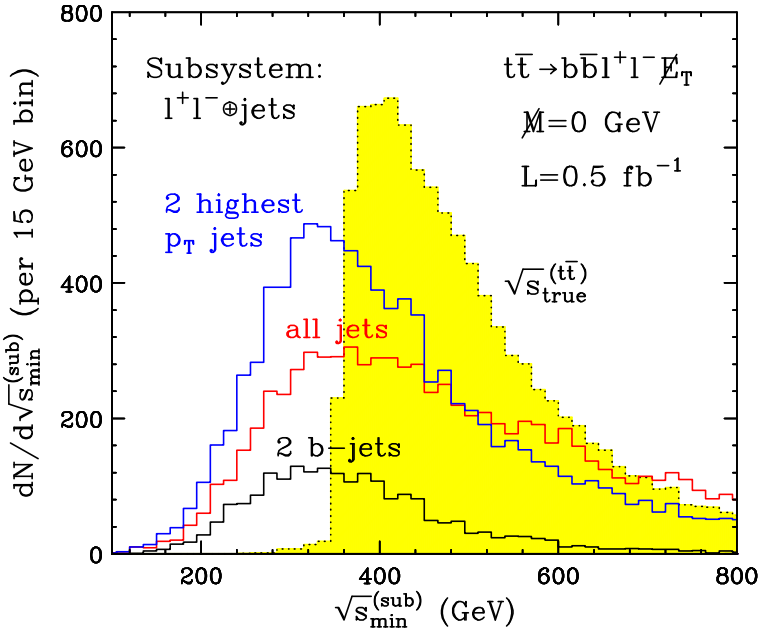

Figure 7. The same as figure 5, but in addition to the two leptons, the subsystem now also includes: exactly two b-tagged jets (black histogram); the two highest p_T jets (blue histogram); or all jets (red histogram). The dotted (yellow-shaded) histogram gives the true $\sqrt{s}$ distribution of the $t\bar{t}$ pair.

gluino pair production in supersymmetry, with each gluino forced to undergo a cascade decay chain involving only QCD jets and nothing else. Note that, to deal with severe combinatorics ref. [12] relied on b-jets from decays through b-squarks and on top of that two leptons from the neutralino decay. Here we replace those leptons with jets so it is a much more challenging situation. For concreteness, we revisit the setup of ref. [1], where two different possibilities for the gluino decays were considered:

- In one scenario, the gluino $\tilde{g}$ is forced to undergo a two-stage cascade decay to the LSP. In the first stage, the gluino decays to the second-lightest neutralino $\tilde{\chi}_2^0$ and two quark jets: $\tilde{g} \to q\bar{q}\tilde{\chi}_2^0$. In turn, $\tilde{\chi}_2^0$ itself is then forced to decay via a 3-body decay to 2 quark jets and the LSP: $\tilde{\chi}_2^0 \to q\bar{q}\tilde{\chi}_1^0$. The resulting gluino signature is 4 jets plus missing energy:

$$\tilde{g} \to jj\tilde{\chi}_2^0 \to jjjj\tilde{\chi}_1^0 \ . \tag{5.1}$$

  Therefore, gluino pair production will nominally result in 8 jet events. Of course, as shown in figure 8, the actual number of reconstructed jets in such events is even higher, due to the effects of ISR, FSR and/or string fragmentation. As seen from the figure, each such event has on average ~ 10 jets, presenting a formidable combinatorics problem. We suspect that all[7] mass reconstruction methods on the market are doomed if they were to face such a scenario. It is therefore of particular interest to

[7]With the possible exception of the M_{Tgen} method of ref. [30], see section 7 below.

JHEP06(2011)041

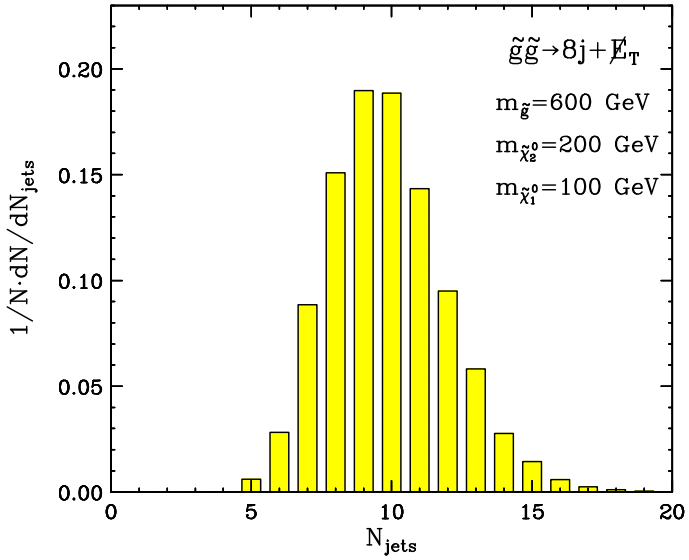

Figure 8. Unit-normalized distribution of jet multiplicity in gluino pair production events, with each gluino decaying to four jets and a $\tilde{\chi}_1^0$ LSP as in (5.1).

see how well the $\sqrt{s}_{\rm min}$ method (which is advertized as universally applicable) would fare under such dire circumstances.

- In the second scenario, the gluino decays directly to the LSP via a three-body decay

$$\tilde{g} \to jj\tilde{\chi}_1^0\,, \tag{5.2}$$

so that gluino pair-production events would nominally have 4 jets and missing energy.

For concreteness, in each scenario we fix the mass spectrum as was done in [1]: we use the approximate gaugino unification relations to relate the gaugino and neutralino masses as

$$m_{\tilde{g}} = 3m_{\tilde{\chi}_2^0} = 6m_{\tilde{\chi}_1^0}\ . \tag{5.3}$$

We can then vary one of these masses, and choose the other two in accord with these relations. Since we assume three-body decays in (5.2) and (5.1), we do not need to specify the SUSY scalar mass parameters, which can be taken to be very large. In addition, as implied by (5.3), we imagine that the lightest two neutralinos are gaugino-like, so that we do not have to specify the higgsino mass parameter either, and it can be taken to be very large as well.

After these preliminaries, our results for these two scenarios are shown in figures 9 and 10, correspondingly. In figure 9 (figure 10) we consider the 8-jet signature arising from (5.1) (the 4-jet signature arising from (5.2)). In both figures, panels (a) correspond to a light mass spectrum $m_{\tilde{g}} = 600\,\text{GeV}$, $m_{\tilde{\chi}_2^0} = 200\,\text{GeV}$ and $m_{\tilde{\chi}_1^0} = 100\,\text{GeV}$; while panels (b) correspond to a heavy mass spectrum $m_{\tilde{g}} = 2400\,\text{GeV}$, $m_{\tilde{\chi}_2^0} = 800\,\text{GeV}$ and $m_{\tilde{\chi}_1^0} = 400\,\text{GeV}$. Each plot shows the same four distributions as in figure 2. The $\sqrt{s}_{\rm min}$ distributions are all plotted for the correct value of the missing mass parameter, namely $\not{M} = 2m_{\tilde{\chi}_1^0}$.

JHEP06(2011)041

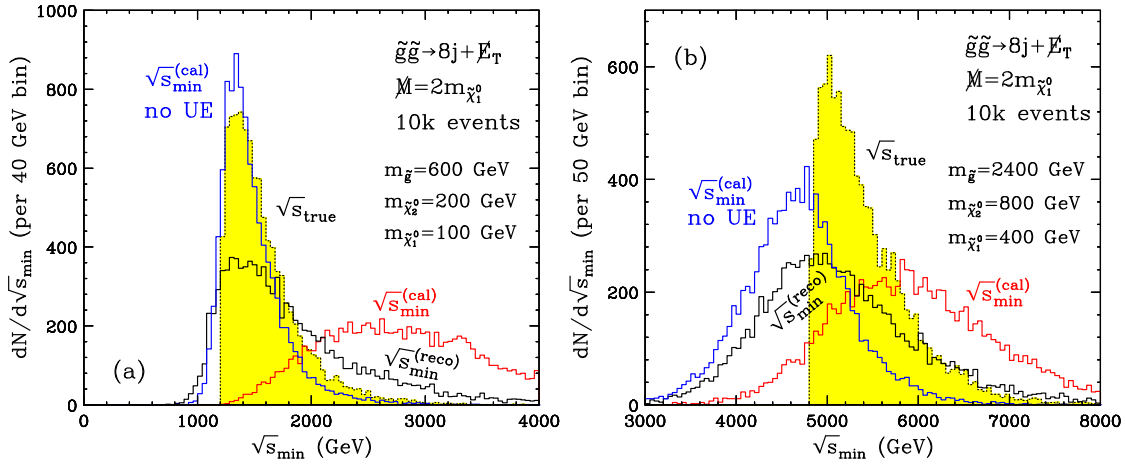

Figure 9. The same as figure 2, but for a SUSY example of gluino pair production, with each gluino decaying to four jets and a $\tilde{\chi}_1^0$ LSP as indicated in (5.1). The mass spectrum is chosen as: (a) $m_{\tilde{g}} = 600\,\text{GeV}$, $m_{\tilde{\chi}_2^0} = 200\,\text{GeV}$ and $m_{\tilde{\chi}_1^0} = 100\,\text{GeV}$; or (b) $m_{\tilde{g}} = 2400\,\text{GeV}$, $m_{\tilde{\chi}_2^0} = 800\,\text{GeV}$ and $m_{\tilde{\chi}_1^0} = 400\,\text{GeV}$. All three $\sqrt{s}_{\text{min}}$ distributions are plotted for the correct value of the missing mass parameter, in this case $\not{M} = 2m_{\tilde{\chi}_1^0}$.

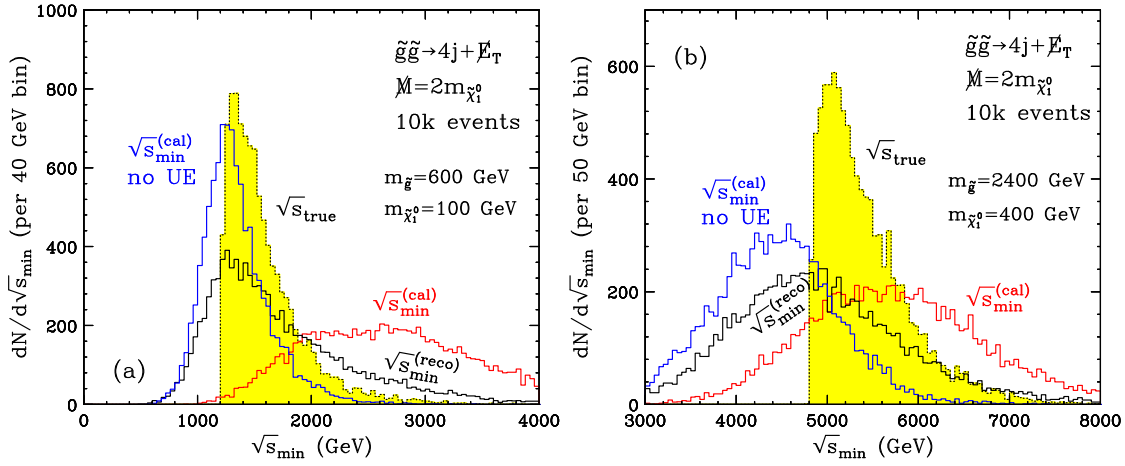

Figure 10. The same as figure 9, but for the case of gluino decays to 2 jets and a $\tilde{\chi}_1^0$ LSP as in (5.2).

Overall, the results seen in figures 9 and 10 are not too different from what we already witnessed in figure 2 for the $t\bar{t}$ example. The (unobservable) distribution $\sqrt{s}_{true}$ shown with the dotted yellow-shaded histogram has a sharp turn-on at the physical mass threshold $M_p = 2m_{\tilde{g}}$. If the effects of the UE are ignored, the position of this threshold is given rather well by the peak of the $\sqrt{s}_{\text{min}}^{(cal)}$ distribution (blue histogram). Unfortunately, the UE shifts the peak in $\sqrt{s}_{\text{min}}^{(cal)}$ by 1-2 TeV (red histogram). Fortunately, the distribution of the RECO-level variable $\sqrt{s}_{\text{min}}^{(reco)}$ (black histogram) is stable against UE contamination, and its peak is still in the right place (near M_p).

JHEP06(2011)041

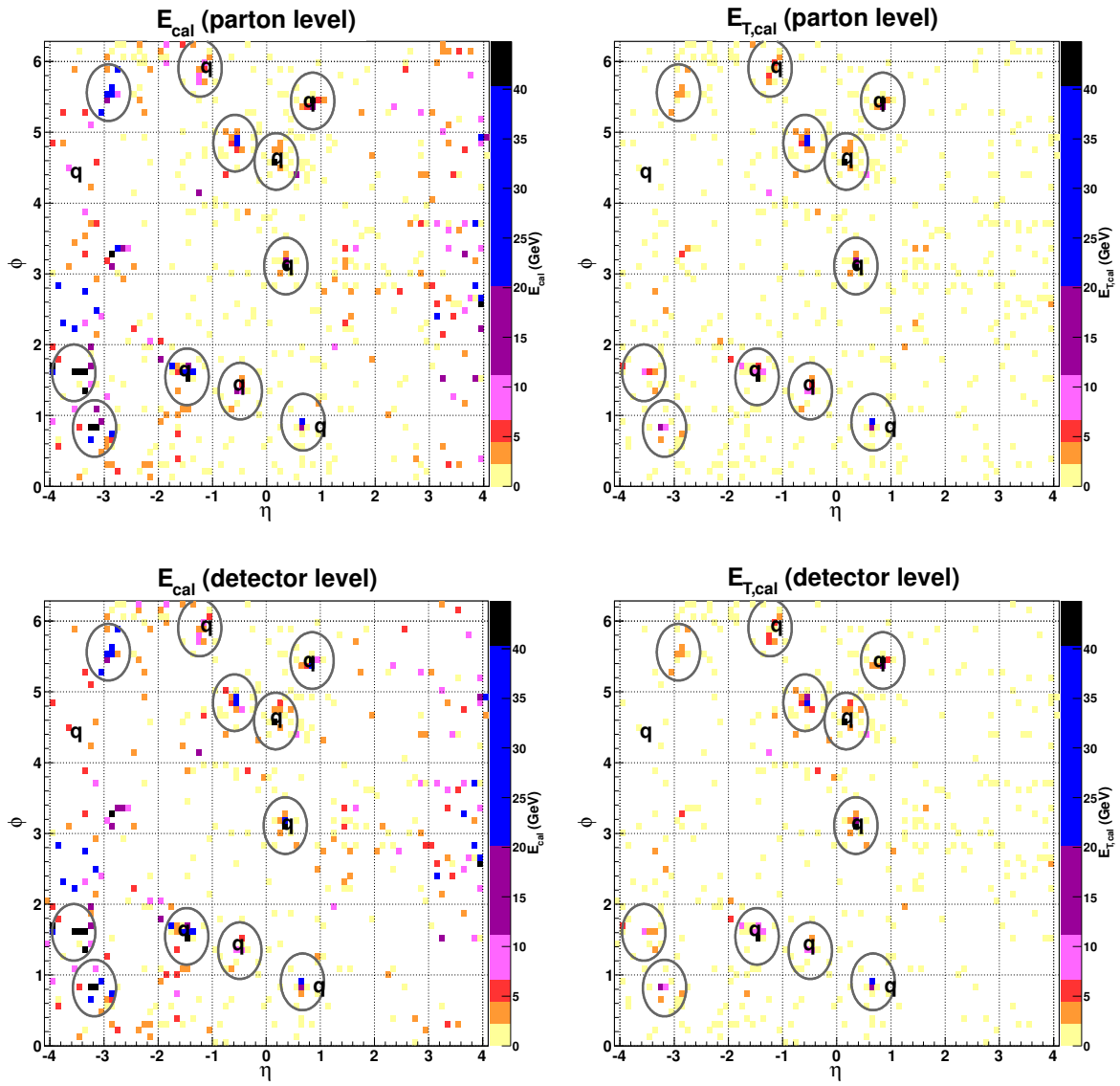

Figure 11. The same as figure 3, but for a SUSY event of gluino pair production, with each gluino forced to decay to 4 jets and the LSP as in (5.1). The SUSY mass spectrum is as in figures 9(a) and 10(a): $m_{\tilde{g}} = 600\,\text{GeV}$, $m_{\tilde{\chi}_2^0} = 200\,\text{GeV}$ and $m_{\tilde{\chi}_1^0} = 100\,\text{GeV}$. As in figures 3 and 4, the circles denote jets reconstructed in PGS, and here "q" marks the location of a quark from a gluino decay chain. Therefore, a circle without a "q" inside corresponds to a jet resulting from ISR or FSR, while a letter "q" without an accompanying circle represents a quark in the gluino decay chain which was not subsequently reconstructed as a jet.

Having already seen a similar behavior in the $t\bar{t}$ example of the previous section, these results may not seem very impressive, until one realizes just how complicated those events are. For illustration, figure 11 shows the previously discussed calorimeter maps for one particular "8 jet" event. This event happens to have 11 reconstructed jets, which is consistent with the typical jet multiplicity seen in figure 8. The values of the $\sqrt{s}$ quantities

JHEP06(2011)041

of interest for this event are listed in table 1. We see that the RECO prescription for calculating $\sqrt{s}_{\rm min}$ is able to compensate for a shift in $\sqrt{s}$ of more than 1.5 TeV! A casual look at figure 11 should be enough to convince the reader just how daunting the task of mass reconstruction in such events is. In this sense, the ease with which the $\sqrt{s}_{\rm min}$ method reveals the gluino mass scale in figures 9 and 10 is quite impressive.

6 An inclusive SUSY example: GMSB study point GM1b

In the Introduction we already mentioned that $\sqrt{s}_{\rm min}$ is a fully inclusive variable. Here we would like to point out that there are two different aspects of the inclusivity property of $\sqrt{s}_{\rm min}$:

- *Object-wise inclusivity:* $\sqrt{s}_{\rm min}$ is inclusive with regards to the type of reconstructed objects. The definition of $\sqrt{s}_{\rm min}^{(reco)}$ does not distinguish between the different types of reconstructed objects (and $\sqrt{s}_{\rm min}^{(cal)}$ makes no reference to any reconstructed objects at all). This makes $\sqrt{s}_{\rm min}$ a very convenient variable to use in those cases where the newly produced particles have many possible decay modes, and restricting oneself to a single exclusive signature would cause loss in statistics. For illustration, consider the gluino pair production example from the previous section. Even though we are always producing the same type of parent particles (two gluinos), in general they can have several different decay modes, leading to a very diverse sample of events with varying number of jets and leptons. Nevertheless, the $\sqrt{s}_{\rm min}^{(reco)}$ distribution, plotted over this whole signal sample, will still be able to pinpoint the gluino mass scale, as explained in section 5.

- *Event-wise inclusivity:* $\sqrt{s}_{\rm min}$ is inclusive also with regards to the type of events, i.e. the type of new particle production. For simplicity, in our previous examples we have been considering only one production mechanism at a time, but this is not really necessary — $\sqrt{s}_{\rm min}$ can also be applied in the case of several simultaneous production mechanisms.

In order to illustrate the last point, in this section we shall consider the simultaneous production of the full spectrum of SUSY particles at a particular benchmark point. We chose the GM1b CMS study point [66], which is nothing but a minimal gauge-mediated SUSY-breaking (GMSB) scenario on the SPS8 Snowmass slope [67]. The input parameters are Λ=80 TeV, M_{mes}=160 TeV, N_{mes}=1, $\tan\beta = 15$ and $\mu > 0$. The physical mass spectrum is given in table 2. Point GM1b is characterized by a neutralino NLSP, which promptly decays (predominantly) to a photon and a gravitino. Therefore, a typical event has two hard photons and missing energy, which provide good handles for suppressing the SM backgrounds.

We now consider inclusive production of all SUSY subprocesses and plot the $\sqrt{s}_{\rm min}$ distributions of interest in figure 12. As usual, the dotted yellow-shaded histogram is the true $\sqrt{s}$ distribution of the parent pair of SUSY particles produced at the top of each decay chain. Since we do not fix the production subprocess, the identity of the parent

JHEP06(2011)041

$\tilde{u}_L$	$\tilde{d}_L$	$\tilde{u}_R$	$\tilde{d}_R$	$\tilde{\ell}_L$	$\tilde{\nu}_\ell$	$\tilde{\ell}_R$	$\tilde{\chi}_2^\pm$	$\tilde{\chi}_4^0$	$\tilde{\chi}_3^0$	$\tilde{g}$
908	911	872	870	289	278	145	371	371	348	690
$\tilde{t}_1$	$\tilde{b}_1$	$\tilde{t}_2$	$\tilde{b}_2$	$\tilde{\tau}_2$	$\tilde{\nu}_\tau$	$\tilde{\tau}_1$	$\tilde{\chi}_1^\pm$	$\tilde{\chi}_2^0$	$\tilde{\chi}_1^0$	$\tilde{G}$
806	863	895	878	290	277	138	206	206	106	0

Table 2. Masses (in GeV) of the SUSY particles at the GM1b study point. Here $\tilde{u}$ and $\tilde{d}$ ($\tilde{\ell}$ and $\tilde{\nu}_\ell$) stand for either of the first two generations squarks (sleptons).

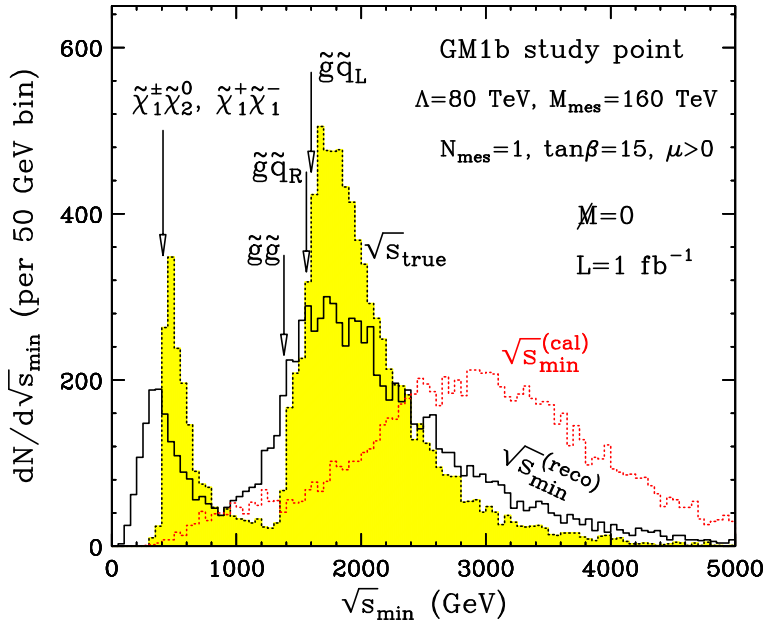

Figure 12. Distribution of the $\sqrt{s}_{\rm min}^{(cal)}$ (dotted red) and $\sqrt{s}_{\rm min}^{(reco)}$ (solid black) variables in inclusive SUSY production for the GMSB GM1a benchmark study point with parameters $\Lambda = 80\,\text{TeV}$, $M_{mes} = 160\,\text{TeV}$, $N_{mes} = 1$, $\tan\beta = 15$ and $\mu > 0$. The dotted yellow-shaded histogram is the true $\sqrt{s}$ distribution of the parent pair of SUSY particles produced at the top of each decay chain (the identity of the parent particles varies from event to event). A few individual mass thresholds are indicated by vertical arrows. The $\sqrt{s}_{\rm min}$ distributions are shown for $\not{M} = 0$ and are normalized to 1 fb^{-1} of data. The vertical arrows mark the mass thresholds for a few dominant SUSY pair-production processes.

particles varies from event to event. Naturally, the most common parent particles are the ones with the highest production cross-sections. For point GM1b, at a 14 TeV LHC, strong SUSY production dominates, and is 87% of the total cross-section. A few of the dominant subprocesses and their cross-sections are listed in table 3.

The true $\sqrt{s}$ distribution in figure 12 exhibits an interesting double-peak structure, which is easy to understand as follows. As we have seen in the exclusive examples from sections 4 and 5, at hadron colliders the particles tend to be produced with $\sqrt{s}$ close to their mass threshold. As seen in table 2, the particle spectrum of the GM1b point can be broadly divided (according to mass) into two groups of superpartners: electroweak sector (the lightest chargino $\tilde{\chi}_1^\pm$, second-to-lightest neutralino $\tilde{\chi}_2^0$ and sleptons) with a mass scale

JHEP06(2011)041

Process	$\tilde{\chi}_1^\pm\tilde{\chi}_2^0$	$\tilde{\chi}_1^+\tilde{\chi}_1^-$	$\tilde{g}\tilde{g}$	$\tilde{g}\tilde{q}_R$	$\tilde{g}\tilde{q}_L$	$\tilde{q}_R\tilde{q}_R$	$\tilde{q}_L\tilde{q}_R$	$\tilde{q}_L\tilde{q}_L$
σ (pb)	0.83	0.43	2.03	2.17	1.90	0.36	0.50	0.28
M_p (GeV)	412	412	1380	~ 1560	~ 1600	~ 1740	~ 1780	~ 1820

Table 3. Cross-sections (in pb) and parent mass thresholds (in GeV) for the dominant production processes at the GM1b study point. The listed squark cross-sections are summed over the light squark flavors and conjugate states. The total SUSY cross-section at point GM1b is 9.4 pb.

on the order of 200 GeV and a strong sector (squarks and gluino) with masses of order $700 - 900$ GeV. The first peak in the true $\sqrt{s}$ distribution (near $\sqrt{s} \sim 500$ GeV) arises from the pair production of two particles from the electroweak sector, while the second, broader peak in the range of $\sqrt{s} \sim 1500 - 2300$ GeV is due to the pair production of two colored superpartners. One may also notice two barely visible bumps (near 950 GeV and 1150 GeV) reflecting the associated production of one colored and one uncolored particle: $\tilde{g}\tilde{\chi}_1^\pm, \tilde{g}\tilde{\chi}_2^0$ and $\tilde{q}\tilde{\chi}_1^\pm, \tilde{q}\tilde{\chi}_2^0$, correspondingly. Each one of those peaks is made up of several contributions from different individual subprocesses, but because their mass thresholds are so close, in the figure they cannot be individually resolved, and appear as a single bump.

If one could somehow directly observe the true $\sqrt{s}$ SUSY distribution (the dotted yellow-shaded histogram in figure 12), this would lead to some very interesting conclusions. First, from the presence of two separate peaks one would know immediately that there are two widely separated scales in the problem. Second, the normalization of each peak would indicate the relative size of the total inclusive cross-sections (in this example, of the particles in the electroweak sector versus those in the strong sector). Finally, the broadness of each peak is indicative of the total number of contributing subprocesses, as well as the typical mass splittings of the particles within each sector. It may appear surprising that one is able to draw so many conclusions from a single distribution of an inclusive variable, but this just comes to show the importance of $\sqrt{s}$ as one of the fundamental collider physics variables.

Unfortunately, because of the missing energy due to the escaping invisible particles, the true $\sqrt{s}$ distribution cannot be observed, and the best one can do to approximate it is to look at the distributions of our inclusive $\sqrt{s}_{\rm min}$ variables discussed in section 2: the calorimeter-based $\sqrt{s}_{\rm min}^{(cal)}$ variable (dotted red histogram in figure 12) and the RECO-level $\sqrt{s}_{\rm min}^{(reco)}$ variable (solid black histogram in figure 12). In the figure, both of those are plotted for $\not{M} = 0$.

First let us concentrate on the calorimeter-based version $\sqrt{s}_{\rm min}^{(cal)}$ (dotted red histogram). We can immediately see the detrimental effects of the UE: first, the electroweak production peak has been almost completely smeared out, while the strong production peak has been shifted upwards by more than a TeV! This behavior is not too surprising, since the same effect was already encountered in our previous examples in sections 4 and 5. Fortunately, we now also know the solution to this problem: one needs to consider the RECO-level variable $\sqrt{s}_{\rm min}^{(reco)}$ instead, which tracks the true $\sqrt{s}$ distribution much better. We can see evidence of this in figure 12 as well: notice how the (black) $\sqrt{s}_{\rm min}^{(reco)}$ histogram exhibits the same features as the (yellow-shaded) true $\sqrt{s}$ distribution. In particular, $\sqrt{s}_{\rm min}^{(reco)}$ does show two separate peaks (indicating that SUSY production takes place at two different

JHEP06(2011)041

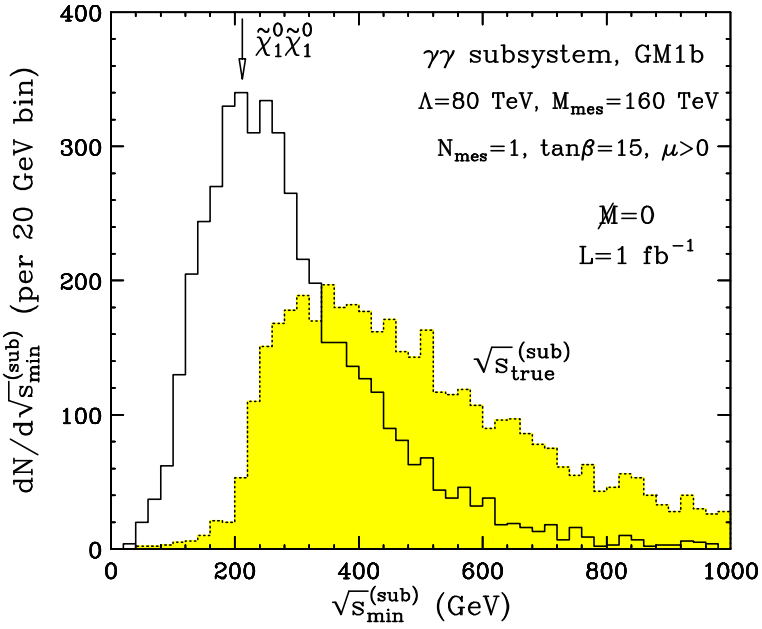

Figure 13. The same as figure 5, but for the GMSB SUSY example considered in figure 12. Here the subsystem is defined in terms of the two hard photons resulting from the two $\tilde{\chi}_1^0 \to \tilde{G} + \gamma$ decays. The vertical arrow marks the onset for inclusive $\tilde{\chi}_1^0\tilde{\chi}_1^0$ production.

mass scales), the peaks are in their proper locations (relative to the missing mass scale $\not{M}$), and have the correct relative width, hinting at the size of the mass splittings in each sector. We thus conclude that all of the interesting physics conclusions that one would be able to reach from looking at the true $\sqrt{s}$ distributions, can still be made based on the inclusive distribution of our RECO-level $\sqrt{s}_{\rm min}^{(reco)}$ variable.

Before concluding this section, we shall take the opportunity to use the GM1b example to also illustrate the $\sqrt{s}_{\rm min}^{(sub)}$ variable proposed in section 3. As already mentioned, the GM1b study point corresponds to a GMSB scenario with a promptly decaying Bino-like $\tilde{\chi}_1^0$ NLSP. Most events therefore contain two hard photons from the two $\tilde{\chi}_1^0$ decays to gravitinos. Then it is quite natural to define the exclusive subsystem in figure 1 in terms of these two photons. The corresponding $\sqrt{s}_{\rm min}^{(sub)}$ distribution is shown in figure 13 with the black solid histogram. For completeness, in the figure we also show the true $\sqrt{s}$ distribution of the $\tilde{\chi}_1^0$ pair (dotted yellow-shaded histogram). The vertical arrow marks the location of the $\tilde{\chi}_1^0\tilde{\chi}_1^0$ mass threshold. We notice that the peak of the $\sqrt{s}_{\rm min}^{(sub)}$ distribution nicely reveals the location of the neutralino mass threshold, and from there the neutralino mass itself. We see that the method of $\sqrt{s}_{\rm min}^{(sub)}$ provides a very simple way of measuring the NLSP mass in such GMSB scenarios (for an alternative approach based on M_{T2}, see [68]).

7 Comparison to other inclusive collider variables

Having discussed the newly proposed variables $\sqrt{s}_{\rm min}^{(reco)}$ and $\sqrt{s}_{\rm min}^{(sub)}$ in various settings in sections 4–6, we shall now compare them to some other global inclusive variables which have been discussed in the literature in relation to determining a mass scale of the new physics.

JHEP06(2011)041

For simplicity here we shall concentrate only on the most model-independent variables, which do not suffer from the topological and combinatorial ambiguities mentioned in the Introduction.

At the moment, there are only a handful of such variables. Depending on the treatment of the unknown masses of the invisible particles, they can be classified into one of the following two categories:

- *Variables which do not depend on an unknown invisible mass parameter.* The most popular members of this class are the "missing H_T" variable

$$\not{H}_T \equiv \left| -\sum_{i=1}^{N_{obj}} \vec{P}_{Ti} \right| , \tag{7.1}$$

  which is simply the magnitude of the $\vec{\not{H}}_T$ vector from eq. (2.8), and the scalar H_T variable which is often called as 'effective mass' $m_{\rm eff}$

$$H_T \equiv \not{H}_T + \sum_{i=1}^{N_{obj}} P_{Ti} \, . \tag{7.2}$$

  Here we follow the notation from section 2, where $\vec{P}_{Ti}$ is the measured transverse momentum of the i-th reconstructed object in the event ($i = 1, 2, \ldots, N_{obj}$). The main advantage of $\not{H}_T$ and H_T is their simplicity: both are very general, and are defined purely in terms of observed quantities, without any unknown mass parameters. The downside of $\not{H}_T$ and H_T is that they cannot be directly correlated with any physical mass scale in a model-independent way.

- *Variables which exhibit dependence on one or more invisible mass parameters.* As two representatives from this class we shall consider M_{Tgen} from ref. [30] and $\sqrt{\hat{s}}_{\rm min}^{(reco)}$ from section 2 here. We remind reader that the M_{Tgen} method assumes exactly two decay chains in each event. The arising combinatorial problem is then solved by brute force — by considering all possible partitions of the event into two sides, computing M_{T2} for each such partition, and taking the minimum value of M_{T2} found in the process. Both M_{Tgen} and $\sqrt{\hat{s}}_{\rm min}^{(reco)}$ introduce a priori unknown parameters related to the mass scale of the missing particles produced in the event. In the case of $\sqrt{\hat{s}}_{\rm min}^{(reco)}$, this is simply the single parameter $\not{M}$, measuring the *total* invisible mass (in the sense of a scalar sum as defined in eq. (1.2)). The M_{Tgen} variable, on the other hand, must in principle introduce two separate missing mass parameters $\not{M}_1$ and $\not{M}_2$ (one for each side of the event). However, the existing applications of M_{Tgen} in the literature have typically made the assumption that $\not{M}_1 = \not{M}_2$, although this is not really necessary and one could just as easily work in terms of two separate inputs $\not{M}_1$ and $\not{M}_2$ [3, 4]. The inconvenience of having to deal with unknown mass parameters in the case of M_{Tgen} and $\sqrt{\hat{s}}_{\rm min}^{(reco)}$ is greatly compensated by the luxury of being able to relate certain features of their distributions to a fundamental physical mass scale in a robust, model-independent way. In particular, the upper *endpoint* $M_{Tgen}^{(max)}$ of the

JHEP06(2011)041

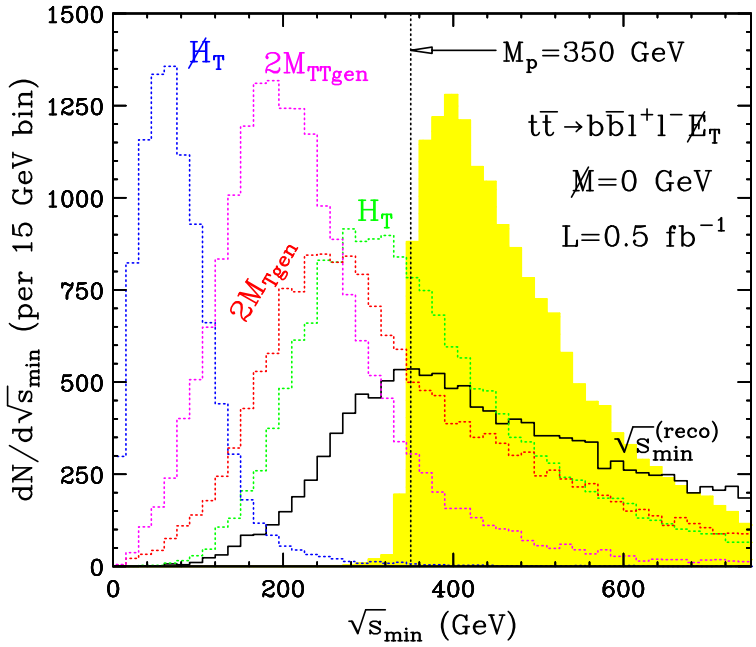

Figure 14. The same as figure 2, but now in addition to the true $\sqrt{s}$ (yellow shaded) and $\sqrt{s}_{\rm min}^{(reco)}$ (black) distribution, we also plot the distributions of $2M_{Tgen}$ (red dots), $2M_{TTgen}$ (magenta dots), H_T (green dots) and $\not{H}_T$ (blue dots), all calculated at the RECO-level. All results include the full simulation of the underlying event. For plotting convenience, the $\not{H}_T$ distribution is shown scaled down by a factor of 2. The vertical dotted line marks the $t\bar{t}$ mass threshold $M_p = 2m_t = 350\,\text{GeV}$.

M_{Tgen} distribution gives the larger of the two parent masses $\max\{M_{P_1}, M_{P_2}\}$ [69]. Therefore, if the two parent masses are the same, i.e. $M_{P_1} = M_{P_2}$, then the parent mass threshold $M_p = M_{P_1} + M_{P_2}$ is simply given by

$$M_p = 2M_{Tgen}^{(max)}. \tag{7.3}$$

On the other hand, as we have already seen in sections 4–6, the *peak* of the $\sqrt{s}_{\rm min}^{(reco)}$ is similarly correlated with the parent mass threshold, see eq. (4.4).

In principle, all four of these variables are inclusive both object-wise and event-wise. It is therefore of interest to compare them with respect to:

1. The degree of correlation with the new physics mass scale M_p.

2. Stability of this correlation against the detrimental effects of the UE.

Figures 14, 15 and 16 allow for such comparisons.

In figure 14 we first revisit the case of the dilepton $t\bar{t}$ sample discussed in section 4. In addition to the true $\sqrt{s}$ (yellow shaded) and $\sqrt{s}_{\rm min}^{(reco)}$ (black) distribution already appearing in figure 2, we now also plot the distributions of $2M_{Tgen}$ (red dots), H_T (green dots) and $\not{H}_T$ (blue dots), all calculated at the RECO-level. For completeness, in figure 14 we also show a variant of M_{Tgen}, called M_{TTgen} (magenta dots), where all visible particle momenta

JHEP06(2011)041

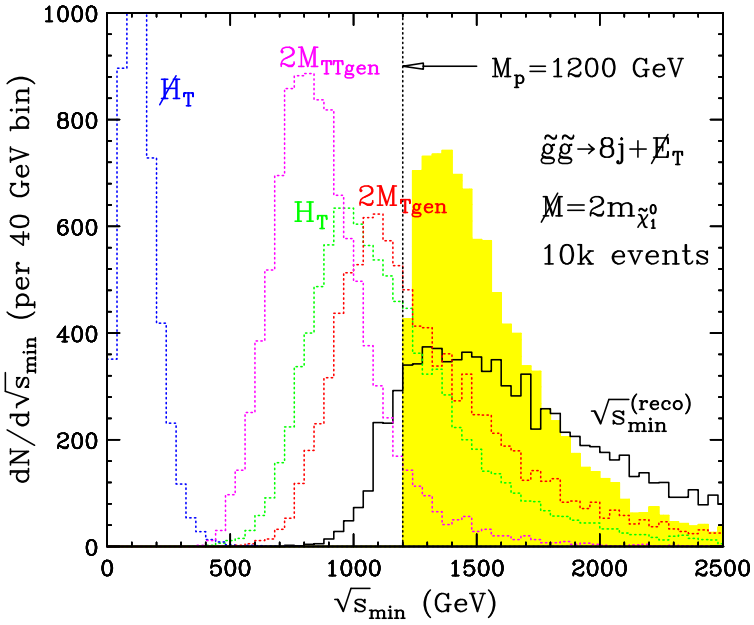

Figure 15. The same as figure 14, but for the gluino pair production example from section 5, with each gluino decaying to 4 jets as in (5.1). We use the light SUSY mass spectrum from figure 9(a). The vertical dotted line now shows the $\tilde{g}\tilde{g}$ mass threshold $M_p = 2m_{\tilde{g}} = 1200\,\text{GeV}$.

are first projected on the transverse plane, before computing M_{Tgen} in the usual way [30].[8] All results include the full simulation of the underlying event. For plotting convenience, the $\not{H}_T$ distribution is shown scaled down by a factor of 2.

Based on the results from figure 14, we can now address the question, which inclusive distribution shows the best correlation with the parent mass scale (in this case the parent mass scale is the $t\bar{t}$ mass threshold $M_p = 2m_t = 350\,\text{GeV}$ marked by the vertical dotted line in figure 14). Let us begin with the two variables, $\not{H}_T$ and H_T, which do not depend on any unknown mass parameters. Figure 14 reveals that the $\not{H}_T$ distribution peaks very far from threshold, and therefore does not reveal much information about the new physics mass scale. Consequently, any attempt at extracting new physics parameters out of the missing energy distribution alone, must make some additional model-dependent assumptions [70]. On the other hand, the H_T distribution appears to correlate better with M_p, since its peak is relatively close to the $t\bar{t}$ threshold. However, this relationship is not in a very controlled way, and it is difficult to know what is the associated systematic error.

Moving on to the variables which carry a dependence on a missing mass parameter, $\sqrt{\hat{s}}_{\text{min}}^{(reco)}$, $2M_{Tgen}$ and $2M_{TTgen}$, we see that all three are affected to some extent by the presence of the UE. In particular, the distributions of $2M_{Tgen}$ and $2M_{TTgen}$ are now smeared and extend significantly beyond their expected endpoint (7.3). Not surprisingly, the UE has a larger impact on $2M_{Tgen}$ than on $2M_{TTgen}$. In either case, there is no obvious endpoint.

[8] We caution the reader that the definition of M_{TTgen} cannot be found in the published version of ref. [30] — the M_{TTgen} discussion was added in a recent replacement on the archive, which appeared more than two years after the original publication.

JHEP06(2011)041

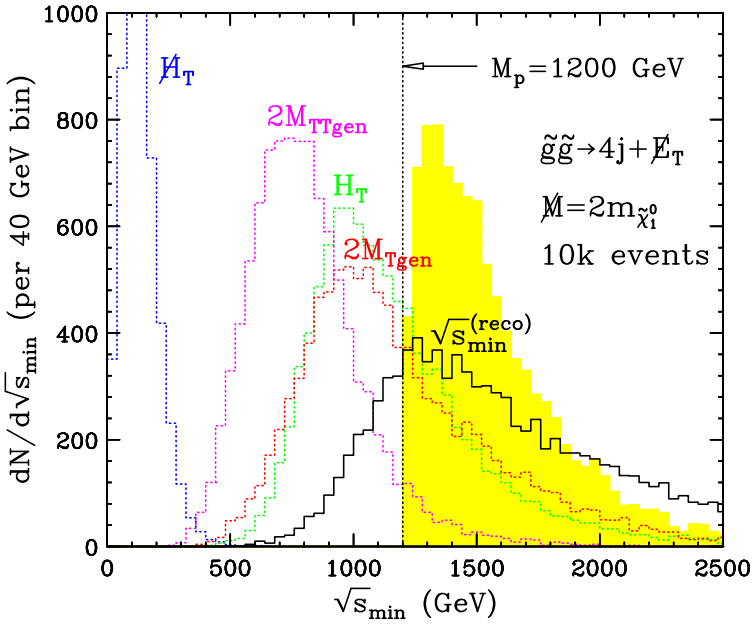

Figure 16. The same as figure 15, but with each gluino decaying to 2 jets as in (5.2). Compare to figure 10(a).

Nevertheless, one could in principle try to extract an endpoint through a straight-line fit, for example, but it is clear that the obtained value will be wrong by a certain amount (depending on the chosen region for fitting and on the associated backgrounds). All these difficulties with $2M_{Tgen}$ and $2M_{TTgen}$ are simply a reflection of the challenge of measuring a mass scale from an endpoint as in (7.3), instead of from a peak as in (4.4). By comparison, the determination of the new physics mass scale from the $\sqrt{s}_{\rm min}^{(reco)}$ distribution is much more robust. As shown in figure 14, the $\sqrt{s}_{\rm min}^{(reco)}$ peak is barely affected by the UE, and is still found precisely in the right location.

All of the above discussion can be directly applied to the SUSY examples considered in section 5 as well. As an illustration, figures 15 and 16 revisit two of the gluino examples from section 5. In both figures, we consider gluino pair-production with a light SUSY spectrum ($m_{\tilde{\chi}_1^0} = 100\,\text{GeV}$, $m_{\tilde{\chi}_2^0} = 200\,\text{GeV}$ and $m_{\tilde{g}} = 600\,\text{GeV}$). Then in figure 15 each gluino decays to 4 jets as in eq. (5.1), while in figure 16 each gluino decays to 2 jets as in eq. (5.2). (Thus figure 15 is the analogue of figure 9(a), while figure 16 is the analogue of figure 10(a).)

The conclusions from figures 15 and 16 are very similar. Both figures confirm that $\not{H}_T$ is not very helpful in determining the gluino mass scale $M_p = 2m_{\tilde{g}} = 1200\,\text{GeV}$ (indicated by the vertical dotted line). The H_T distribution, on the other hand, has a nice well-defined peak, but the location of the H_T peak always underestimates the gluino mass scale (by about 250 GeV in each case). Figures 15 and 16 also confirm the effect already seen in figure 14: that the underlying event causes the $2M_{Tgen}$ and $2M_{TTgen}$ distributions to extend well beyond their upper kinematic endpoint, thus violating (7.3) and making the corresponding extraction of M_p rather problematic. In fact, just by looking

JHEP06(2011)041

at figures 15 and 16, one might be tempted to deduce that, if anything, it is the *peak* in $2M_{Tgen}$ that perhaps might indicate the value of the new physics mass scale and not the $2M_{Tgen}$ endpoint. Finally, the $\sqrt{s}_{\rm min}^{(reco)}$ distribution also feels to some extent the effects from the UE, but always has its peak in the near vicinity of M_p. Therefore, among the five inclusive variables under consideration here, $\sqrt{s}_{\rm min}^{(reco)}$ appears to provide the best estimate of the new physics mass scale. The correlation (4.4) advertized in this paper is seen to hold very well in figure 16 and reasonably well in figure 15.

8 Summary and conclusions

Since the original proposal of the $\sqrt{s}_{\rm min}$ variable in ref. [1], its practicability has been called into question in light of the effects from the underlying event, in particular initial state radiation and multiple parton interactions. In this paper we proposed two variations of the $\sqrt{s}_{\rm min}$ variable which are intended to avoid this problems.

1. *RECO-level* $\sqrt{s}_{\rm min}^{(reco)}$. The first variant, the RECO-level variable $\sqrt{s}_{\rm min}^{(reco)}$ introduced in section 2, is basically a modification of the *prescription for computing* the original $\sqrt{s}_{\rm min}$ variable: instead of using (muon-corrected) calorimeter deposits, as was done in [1, 41], one could instead calculate $\sqrt{s}_{\rm min}$ with the help of the reconstructed objects (jets and isolated photons, electrons and muons). Our examples in sections 4, 5 and 6 showed that this procedure tends to automatically subtract out the bulk of the UE contributions, rendering the $\sqrt{s}_{\rm min}^{(reco)}$ variable safe.

2. *Subsystem* $\sqrt{s}_{\rm min}^{(sub)}$. Our second suggestion, discussed in section 3, was to apply $\sqrt{s}_{\rm min}$ to a *subsystem* of the observed event, which is suitably defined so that it does not include the contributions from the underlying event. The easiest way to do this is to veto jets from entering the definition of the subsystem. In this case, the subsystem variable $\sqrt{s}_{\rm min}^{(sub)}$ is completely unaffected by the underlying event. However, depending on the particular scenario, in principle one could also allow (certain kinds of) jets to enter the subsystem. As long as there is an efficient method (through cuts) of selecting jets which (most likely) did not originate from the UE, this should work as well, as demonstrated in figure 5 with our $t\bar{t}$ example.

Being simply variants of the original $\sqrt{s}_{\rm min}$ variable, both $\sqrt{s}_{\rm min}^{(reco)}$ and $\sqrt{s}_{\rm min}^{(sub)}$ automatically inherit the many nice properties of $\sqrt{s}_{\rm min}$:

- Both $\sqrt{s}_{\rm min}^{(reco)}$ and $\sqrt{s}_{\rm min}^{(sub)}$ have a clear physical meaning: the minimum CM energy in the (sub)system, which is required in order to explain the observed signal in the detector.

- Both $\sqrt{s}_{\rm min}^{(reco)}$ and $\sqrt{s}_{\rm min}^{(sub)}$ are defined in a manifestly 1+3 Lorentz invariant way. As a consequence, their definitions utilize the available information about the longitudinal momentum components of the particles observed in the detector.

- Both $\sqrt{s}_{\rm min}^{(reco)}$ and $\sqrt{s}_{\rm min}^{(sub)}$ can be computed by simple analytical formulas, eqs. (2.5), (2.6) and (3.1)–(3.4), correspondingly.

JHEP06(2011)041

- $\sqrt{s}_{\min}^{(reco)}$ (and to some extent $\sqrt{s}_{\min}^{(sub)}$) is a general, global, and inclusive variable, which can be applied to *any* type of events, regardless of the event topology, number or type of reconstructed objects, number or type of missing particles, etc. For example, all of the arbitrariness associated with the number and type of missing particles is encoded by a *single* parameter $\not{M}$.

- The most important property of both $\sqrt{s}_{\min}^{(reco)}$ and $\sqrt{s}_{\min}^{(sub)}$ is that they exhibit a *peak* in their distributions, which *correlates* with the mass scale M_p of the parent particles. In this regard we remind the reader that, compared to a kinematic endpoint, a peak is a feature which is much easier to observe and subsequently measure precisely over the SM backgrounds. This point was specifically illustrated in section 7, where we contrasted the observability of the peak in the $\sqrt{s}_{\min}^{(reco)}$ distribution to the observability of the endpoints of the $2M_{Tgen}$ and $2M_{TTgen}$ distributions.

At the same time, compared to the original calorimeter-based $\sqrt{s}_{\min}$ variable considered in ref. [1], the new variables $\sqrt{s}_{\min}^{(reco)}$ and $\sqrt{s}_{\min}^{(sub)}$ proposed here have one crucial advantage: they have very little sensitivity to the effects from the underlying event (ISR and MPI). As a result, the measurement of the corresponding mass scale from the peak in the distribution of $\sqrt{s}_{\min}^{(reco)}$ or $\sqrt{s}_{\min}^{(sub)}$ is robust and physically meaningful.

Acknowledgments

We thank A. Barr, C. Lester, F. Moortgat, L. Pape and B. Webber for stimulating discussions and correspondence. This work is supported in part by a US Department of Energy grant DE-FG02-97ER41029. SLAC is operated by Stanford University for the US Department of Energy under contract DE-AC02-76SF00515.

References

[1] P. Konar, K. Kong and K.T. Matchev, $\sqrt{\hat{s}}_{\min}$*: A Global inclusive variable for determining the mass scale of new physics in events with missing energy at hadron colliders*, *JHEP* **03** (2009) 085 [arXiv:0812.1042] [SPIRES].

[2] S. Chang and A. de Gouvêa, *Neutrino alternatives for missing energy events at colliders*, *Phys. Rev.* **D 80** (2009) 015008 [arXiv:0901.4796] [SPIRES].

[3] A.J. Barr, B. Gripaios and C.G. Lester, *Transverse masses and kinematic constraints: from the boundary to the crease*, *JHEP* **11** (2009) 096 [arXiv:0908.3779] [SPIRES].

[4] P. Konar, K. Kong, K.T. Matchev and M. Park, *Dark Matter Particle Spectroscopy at the LHC: Generalizing MT2 to Asymmetric Event Topologies*, *JHEP* **04** (2010) 086 [arXiv:0911.4126] [SPIRES].

JHEP06(2011)041

[5] K. Agashe, D. Kim, M. Toharia and D.G.E. Walker, *Distinguishing Dark Matter Stabilization Symmetries Using Multiple Kinematic Edges and Cusps*, *Phys. Rev.* **D 82** (2010) 015007 [arXiv:1003.0899] [SPIRES].

[6] A.J. Barr and C.G. Lester, *A Review of the Mass Measurement Techniques proposed for the Large Hadron Collider*, *J. Phys.* **G 37** (2010) 123001 [arXiv:1004.2732] [SPIRES].

[7] I. Hinchliffe, F.E. Paige, M.D. Shapiro, J. Soderqvist and W. Yao, *Precision SUSY measurements at CERN LHC*, *Phys. Rev.* **D 55** (1997) 5520 [hep-ph/9610544] [SPIRES].

[8] H. Bachacou, I. Hinchliffe and F.E. Paige, *Measurements of masses in SUGRA models at CERN LHC*, *Phys. Rev.* **D 62** (2000) 015009 [hep-ph/9907518] [SPIRES].

[9] I. Hinchliffe and F.E. Paige, *Measurements in SUGRA models with large* $\tan\beta$ *at LHC*, *Phys. Rev.* **D 61** (2000) 095011 [hep-ph/9907519] [SPIRES].

[10] B.C. Allanach, C.G. Lester, M.A. Parker and B.R. Webber, *Measuring sparticle masses in non-universal string inspired models at the LHC*, *JHEP* **09** (2000) 004 [hep-ph/0007009] [SPIRES].

[11] B.K. Gjelsten, D.J. Miller, 2 and P. Osland, *Measurement of SUSY masses via cascade decays for SPS 1a*, *JHEP* **12** (2004) 003 [hep-ph/0410303] [SPIRES].

[12] B.K. Gjelsten, D.J. Miller, 2 and P. Osland, *Measurement of the gluino mass via cascade decays for SPS 1a*, *JHEP* **06** (2005) 015 [hep-ph/0501033] [SPIRES].

[13] A. Birkedal, R.C. Group and K. Matchev, *Slepton mass measurements at the LHC*, hep-ph/0507002 [SPIRES].

[14] D.J. Miller, 2, P. Osland and A.R. Raklev, *Invariant mass distributions in cascade decays*, *JHEP* **03** (2006) 034 [hep-ph/0510356] [SPIRES].

[15] M. Burns, K. Kong, K.T. Matchev and M. Park, *A General Method for Model-Independent Measurements of Particle Spins, Couplings and Mixing Angles in Cascade Decays with Missing Energy at Hadron Colliders*, *JHEP* **10** (2008) 081 [arXiv:0808.2472] [SPIRES].

[16] D. Costanzo and D.R. Tovey, *Supersymmetric particle mass measurement with invariant mass correlations*, *JHEP* **04** (2009) 084 [arXiv:0902.2331] [SPIRES].

[17] M. Burns, K.T. Matchev and M. Park, *Using kinematic boundary lines for particle mass measurements and disambiguation in SUSY-like events with missing energy*, *JHEP* **05** (2009) 094 [arXiv:0903.4371] [SPIRES].

[18] K.T. Matchev, F. Moortgat, L. Pape and M. Park, *Precise reconstruction of sparticle masses without ambiguities*, *JHEP* **08** (2009) 104 [arXiv:0906.2417] [SPIRES].

[19] M.M. Nojiri, G. Polesello and D.R. Tovey, *Proposal for a new reconstruction technique for SUSY processes at the LHC*, hep-ph/0312317 [SPIRES].

[20] K. Kawagoe, M.M. Nojiri and G. Polesello, *A new SUSY mass reconstruction method at the CERN LHC*, *Phys. Rev.* **D 71** (2005) 035008 [hep-ph/0410160] [SPIRES].

[21] H.-C. Cheng, J.F. Gunion, Z. Han, G. Marandella and B. McElrath, *Mass Determination in SUSY-like Events with Missing Energy*, *JHEP* **12** (2007) 076 [arXiv:0707.0030] [SPIRES].

[22] M.M. Nojiri, G. Polesello and D.R. Tovey, *A hybrid method for determining SUSY particle masses at the LHC with fully identified cascade decays*, *JHEP* **05** (2008) 014 [arXiv:0712.2718] [SPIRES].

JHEP06(2011)041

[23] H.-C. Cheng, D. Engelhardt, J.F. Gunion, Z. Han and B. McElrath, *Accurate Mass Determinations in Decay Chains with Missing Energy*, *Phys. Rev. Lett.* **100** (2008) 252001 [arXiv:0802.4290] [SPIRES].

[24] H.-C. Cheng, J.F. Gunion, Z. Han and B. McElrath, *Accurate Mass Determinations in Decay Chains with Missing Energy: II*, *Phys. Rev.* **D 80** (2009) 035020 [arXiv:0905.1344] [SPIRES].

[25] B. Webber, *Mass determination in sequential particle decay chains*, *JHEP* **09** (2009) 124 [arXiv:0907.5307] [SPIRES].

[26] M.M. Nojiri, K. Sakurai and B.R. Webber, *Reconstructing particle masses from pairs of decay chains*, *JHEP* **06** (2010) 069 [arXiv:1005.2532] [SPIRES].

[27] M. Burns, K. Kong, K.T. Matchev and M. Park, *Using Subsystem MT2 for Complete Mass Determinations in Decay Chains with Missing Energy at Hadron Colliders*, *JHEP* **03** (2009) 143 [arXiv:0810.5576] [SPIRES].

[28] C.G. Lester and D.J. Summers, *Measuring masses of semiinvisibly decaying particles pair produced at hadron colliders*, *Phys. Lett.* **B 463** (1999) 99 [hep-ph/9906349] [SPIRES].

[29] A. Barr, C. Lester and P. Stephens, *m(T2) : The Truth behind the glamour*, *J. Phys.* **G 29** (2003) 2343 [hep-ph/0304226] [SPIRES].

[30] C. Lester and A. Barr, *MTGEN : Mass scale measurements in pair-production at colliders*, *JHEP* **12** (2007) 102 [arXiv:0708.1028] [SPIRES].

[31] W.S. Cho, K. Choi, Y.G. Kim and C.B. Park, *Gluino Stransverse Mass*, *Phys. Rev. Lett.* **100** (2008) 171801 [arXiv:0709.0288] [SPIRES].

[32] B. Gripaios, *Transverse Observables and Mass Determination at Hadron Colliders*, *JHEP* **02** (2008) 053 [arXiv:0709.2740] [SPIRES].

[33] A.J. Barr, B. Gripaios and C.G. Lester, *Weighing Wimps with Kinks at Colliders: Invisible Particle Mass Measurements from Endpoints*, *JHEP* **02** (2008) 014 [arXiv:0711.4008] [SPIRES].

[34] W.S. Cho, K. Choi, Y.G. Kim and C.B. Park, *Measuring superparticle masses at hadron collider using the transverse mass kink*, *JHEP* **02** (2008) 035 [arXiv:0711.4526] [SPIRES].

[35] H.-C. Cheng and Z. Han, *Minimal Kinematic Constraints and MT2*, *JHEP* **12** (2008) 063 [arXiv:0810.5178] [SPIRES].

[36] K.T. Matchev, F. Moortgat, L. Pape and M. Park, *Precision sparticle spectroscopy in the inclusive same- sign dilepton channel at LHC*, *Phys. Rev.* **D 82** (2010) 077701 [arXiv:0909.4300] [SPIRES].

[37] P. Konar, K. Kong, K.T. Matchev and M. Park, *Superpartner Mass Measurement Technique using 1D Orthogonal Decompositions of the Cambridge Transverse Mass Variable M_{T2}*, *Phys. Rev. Lett.* **105** (2010) 051802 [arXiv:0910.3679] [SPIRES].

[38] D.R. Tovey, *On measuring the masses of pair-produced semi-invisibly decaying particles at hadron colliders*, *JHEP* **04** (2008) 034 [arXiv:0802.2879] [SPIRES].

[39] G. Polesello and D.R. Tovey, *Supersymmetric particle mass measurement with the boost-corrected contransverse mass*, *JHEP* **03** (2010) 030 [arXiv:0910.0174] [SPIRES].

[40] K.T. Matchev and M. Park, *A general method for determining the masses of semi- invisibly decaying particles at hadron colliders*, arXiv:0910.1584 [SPIRES].

JHEP06(2011)041

[41] A. Papaefstathiou and B. Webber, *Effects of QCD radiation on inclusive variables for determining the scale of new physics at hadron colliders*, *JHEP* **06** (2009) 069 [arXiv:0903.2013] [SPIRES].

[42] A. Papaefstathiou and B. Webber, *Effects of invisible particle emission on global inclusive variables at hadron colliders*, *JHEP* **07** (2010) 018 [arXiv:1004.4762] [SPIRES].

[43] New Physics Working Group collaboration, G. Brooijmans et al., *New Physics at the LHC. A Les Houches Report: Physics at TeV Colliders 2009 - New Physics Working Group*, arXiv:1005.1229 [SPIRES].

[44] Greg Landsberg, $\not{E}_T$ *in CMS*, talk given at the *Missing Energy* workshop, UC Davis, April 1, 2009.

[45] U. Baur, T. Plehn and D.L. Rainwater, *Determining the Higgs boson selfcoupling at hadron colliders*, *Phys. Rev.* **D 67** (2003) 033003 [hep-ph/0211224] [SPIRES].

[46] T. Han, *Collider phenomenology: Basic knowledge and techniques*, hep-ph/0508097 [SPIRES].

[47] A.J. Barr, B. Gripaios and C.G. Lester, *Measuring the Higgs boson mass in dileptonic W-boson decays at hadron colliders*, *JHEP* **07** (2009) 072 [arXiv:0902.4864] [SPIRES].

[48] J.M. Butterworth, A.R. Davison, M. Rubin and G.P. Salam, *Jet substructure as a new Higgs search channel at the LHC*, *Phys. Rev. Lett.* **100** (2008) 242001 [arXiv:0802.2470] [SPIRES].

[49] S.D. Ellis, C.K. Vermilion and J.R. Walsh, *Techniques for improved heavy particle searches with jet substructure*, *Phys. Rev.* **D 80** (2009) 051501 [arXiv:0903.5081] [SPIRES].

[50] S.D. Ellis, C.K. Vermilion and J.R. Walsh, *Recombination Algorithms and Jet Substructure: Pruning as a Tool for Heavy Particle Searches*, *Phys. Rev.* **D 81** (2010) 094023 [arXiv:0912.0033] [SPIRES].

[51] D. Krohn, J. Thaler and L.-T. Wang, *Jet Trimming*, *JHEP* **02** (2010) 084 [arXiv:0912.1342] [SPIRES].

[52] D. Krohn, L. Randall and L.-T. Wang, *On the Feasibility and Utility of ISR Tagging*, arXiv:1101.0810 [SPIRES].

[53] J. Alwall, K. Hiramatsu, M.M. Nojiri and Y. Shimizu, *Novel reconstruction technique for New Physics processes with initial state radiation*, *Phys. Rev. Lett.* **103** (2009) 151802 [arXiv:0905.1201] [SPIRES].

[54] M.M. Nojiri and K. Sakurai, *Controlling ISR in sparticle mass reconstruction*, *Phys. Rev.* **D 82** (2010) 115026 [arXiv:1008.1813] [SPIRES].

[55] J. Alwall et al., *Comparative study of various algorithms for the merging of parton showers and matrix elements in hadronic collisions*, *Eur. Phys. J.* **C 53** (2008) 473 [arXiv:0706.2569] [SPIRES].

[56] J. Alwall, A. Freitas and O. Mattelaer, *The Matrix Element Method and QCD Radiation*, *Phys. Rev.* **D 83** (2011) 074010 [arXiv:1010.2263] [SPIRES].

[57] T. Plehn, D. Rainwater and P.Z. Skands, *Squark and gluino production with jets*, *Phys. Lett.* **B 645** (2007) 217 [hep-ph/0510144] [SPIRES].

[58] J. Alwall, S. de Visscher and F. Maltoni, *QCD radiation in the production of heavy colored particles at the LHC*, *JHEP* **02** (2009) 017 [arXiv:0810.5350] [SPIRES].

JHEP06(2011)041

[59] J. Alwall, M.-P. Le, M. Lisanti and J.G. Wacker, *Searching for Directly Decaying Gluinos at the Tevatron*, *Phys. Lett.* **B 666** (2008) 34 [arXiv:0803.0019] [SPIRES].

[60] J. Alwall, M.-P. Le, M. Lisanti and J.G. Wacker, *Model-Independent Jets plus Missing Energy Searches*, *Phys. Rev.* **D 79** (2009) 015005 [arXiv:0809.3264] [SPIRES].

[61] T. Sjöstrand, S. Mrenna and P.Z. Skands, *PYTHIA 6.4 Physics and Manual*, *JHEP* **05** (2006) 026 [hep-ph/0603175] [SPIRES].

[62] J. Conway, *PGS: Simple simulation package for generic collider detectors*, http://www.physics.ucdavis.edu/~conway/research/software/pgs/pgs.html.

[63] CMS collaboration, G.L. Bayatian et al., *CMS physics: Technical design report, vol. I: "Detector Performance and Software*, CERN-LHC- 2006-001.

[64] N. Kidonakis, *Next-to-next-to-leading soft-gluon corrections for the top quark cross section and transverse momentum distribution*, *Phys. Rev.* **D 82** (2010) 114030 [arXiv:1009.4935] [SPIRES].

[65] P. Konar, K. Kong, K.T. Matchev and M. Park, in preparation.

[66] https://twiki.cern.ch/twiki/bin/view/Main/SezenSekmen.

[67] B.C. Allanach et al., *The Snowmass points and slopes: Benchmarks for SUSY searches*, *Eur. Phys. J.* **C 25** (2002) 113 [hep-ph/0202233] [SPIRES].

[68] K. Hamaguchi, E. Nakamura and S. Shirai, *A Measurement of Neutralino Mass at the LHC in Light Gravitino Scenarios*, *Phys. Lett.* **B 666** (2008) 57 [arXiv:0805.2502] [SPIRES].

[69] A.J. Barr and C. Gwenlan, *The race for supersymmetry: using mT2 for discovery*, *Phys. Rev.* **D 80** (2009) 074007 [arXiv:0907.2713] [SPIRES].

[70] J. Hubisz, J. Lykken, M. Pierini and M. Spiropulu, *Missing energy look-alikes with 100 pb-1 at the LHC*, *Phys. Rev.* **D 78** (2008) 075008 [arXiv:0805.2398] [SPIRES].

JHEP06(2011)041